Research Article

Human Umbilical Cord Perivascular Cells Prevent Tumor Growth in a Melanoma Tumor-Bearing Mouse Model and Modulate Breast Cancer and Melanoma Cells in a Cell Line-Dependent Manner *In Vitro*

Lianet Lopez [ID],[1] **Hannah Shuster-Hyman** [ID],[1,2] **Eden Marco** [ID],[1] **Hasna Khan** [ID],[1] **Avishai Gasner** [ID],[1,3] **Aleksandra Uzelac**,[1] **Brandon Wyse** [ID],[1] **Poonam Mander** [ID],[1] **Mugundhine Sangaralingam** [ID],[1] **Joseph Fish**,[1] **Ariel Gorodensky** [ID],[1] **Samar Mouazz**,[1] **Amanda Kauffman** [ID],[1] **Denis Gallagher** [ID],[1] **Andrée Gauthier-Fisher** [ID],[1] and **Clifford L. Librach** [ID][1,2,3,4,5]

[1]*CReATe Fertility Centre, Toronto, Ontario, Canada*
[2]*Institute of Medical Sciences, University of Toronto, Toronto, Canada*
[3]*Department of Physiology, University of Toronto, Toronto, Canada*
[4]*Department of Obstetrics & Gynecology, University of Toronto, Toronto, Canada*
[5]*Sunnybrook Research Institute, Toronto, Ontario, Canada*

Correspondence should be addressed to Andrée Gauthier-Fisher; andree@createivf.com and
Clifford L. Librach; drlibrach@createivf.com

First trimester (FTM) and term human umbilical cord perivascular cells are promising mesenchymal stromal cell candidates to mitigate side effects of oncotherapy, but their safety for cancer patients remains to be determined. This study was designed to determine if human umbilical cord perivascular cells modulate tumor growth when injected systemically in a tumor-bearing mouse model. Immunodeficient mice-bearing palpable subcutaneous SK-MEL-28 human melanoma tumors were randomized to receive a tail vein injection of three human umbilical cord perivascular cell lines resuspended in hank's buffer saline solution (vehicle) or vehicle only, as a control. Fibroblast cells were included as a cell control in some experiments. Tumor size was monitored weekly and weighed at 3-weeks postinjection. Cell fate and tumor cell proliferation, apoptosis, vascularization as well as tumor-associated immune cells were assessed using immunostaining and flow cytometry. Serum tumor necrosis factor alpha and C-reactive protein levels were measured using enzyme-linked immunosorbent assays. Transwell coculture models were used to study the paracrine effects of multiple lines of human umbilical cord cells on human melanoma cell lines as well as breast cancer cell lines. Systemic administration of FTM and term human umbilical cord perivascular cells, but not fibroblast cells, prevented melanoma tumor growth in a tumor-bearing animal model by modulating tumor cell proliferation and systemic inflammatory mechanisms. Cancer cell- and donor-dependent paracrine effects on cancer cell growth were observed *in vitro*. Our preclinical studies thus suggest that, with regards to its effects on tumor growth, systemic administration of FTM and term human umbilical cord perivascular cells may be a safe cell therapy to address the side effects of cancer.

1. Introduction

While cancer remains one of the major causes of death in the developed world, mortality rates following diagnosis continue to decline [1], and the need to address the side effects of cancer treatments that affect survivors' quality of life is growing. Long-term side effects of chemotherapy such as gastrointestinal dysfunction, cardiovascular disease, and neurotoxicity may arise, and can have a lasting impact on survivors [2]. In prepubescent and reproductive-aged patients, the gonadotoxic effects of cancer treatments can result in infertility and an overall decline in health resulting from gonadal dysfunction [3]. In recent years,

female breast cancer has become the most diagnosed cancer, accounting for 11.7% of all cancers [4]. The incidence of melanoma among reproductive-aged adults is increasing as well [5]. These cancers have among the highest survival rates (93% and 90%, respectively) [1].

Mesenchymal stromal cells (MSC), which are nonhematopoietic cells that can be isolated and expanded from most vascularized tissues in the body, have been widely studied for their regenerative properties and potential use for cell therapy due to their multipotency, immune privilege, and immunomodulatory potential [6–8]. As such, MSCs represent a promising treatment option for preserving fertility and gonadal as well as other tissue function in cancer survivors. However, inconsistent literature findings suggest that MSC may also have a direct impact (stimulatory or inhibitory) on cancer growth [9–11]. With regards to melanoma, the circum-tumor injection of adipose tissue-derived MSC (AT-MSC) was shown to reduce tumor growth in human melanoma-bearing mice over a 30-day period [12]. In addition, the intravenous (IV) or intratumoral injection of bone marrow-derived (BM)-MSC reduced melanoma tumor volume in mice over a three-week period, with IV injection demonstrating more significant reductions [13]. Such studies highlight the antitumor effects of MSC, however dozens of studies utilizing various cancer cells and MSC sources have been reported, and the effects of MSC on tumor growth remain unclear and appear to be dependent on the cancer type, source of MSC, and the route and timing of MSC delivery [11]. Given the discordant findings in the published literature, further work is needed to examine the effects of MSC from various sources on tumor growth before they can be considered a therapeutic option in oncological indications.

Human umbilical cord perivascular cells (HUCPVC) are derived from the perivascular region of first trimester (FTM) or term umbilical cords and are one of the richest known sources of MSC. HUCPVC are isolated noninvasively and may be a good allogeneic cell therapy candidate, exhibiting a superior expansion capacity and a higher degree of immune privilege, compared to bone marrow-derived (BM-) MSC [14–16]. In general, HUCPVC express high levels of markers associated with an MSC phenotype (CD90, CD44, CD73, and CD105) and a subpopulation of these cells express pericyte-associated markers CD146 and PDGFRbeta, as well as immunoprivilege-associated molecule HLA-G in culture, albeit to varying levels [8, 17–20]. Additionally, HUCPVC show significant multilineage differentiation and proliferation capacity in culture, and their paracrine and immunomodulatory properties have been well characterized. This includes the expression of dozens of cytokines and chemokines with pleiotropic effects [8, 18, 20–23]. Previous studies from our group have shown that FTM HUCPVC have superior regenerative and angiogenic properties compared to term HUCPVC [16, 17, 24]. We have also previously shown that FTM and term HUCPVC retain their phenotypical, proliferative, multipotent, and regenerative properties (paracrine profiles) when exposed to alkylating chemotherapeutics [18]. Finally, our previous data suggest that HUCPVC can prevent fertility loss in male and female

models of chemotherapy-induced gonadal damage [18, 23]. As such they are a promising candidate for regenerative cell therapy to mitigate side effects of cancer treatments in oncology patients, including for fertility preservation [25]. This leads to the rationale that FTM and term HUCPVC could be used as an adjunct therapy to prevent side effects of cancer therapy, should they prove to be safe with regards to their effect on cancer cells themselves, which remains to be tested. Further published work showed that IV-delivered HUCPVC interact directly with immune cells such as neutrophils and macrophages in the lungs within minutes of their injection. The rapid clearance of HUCPVC by immune cells in the lungs leads to polarization of macrophages from pro- to anti-inflammatory phenotypes, reduced circulation of proinflammatory monocytes and modulation of inflammatory mediators (IL-6, tumor necrosis factor alpha [TNF-α]) and related signaling pathways in the circulation and in distal tissue such as the brain, ultimately leading to neuroprotective and beneficial behavioral effects [8, 26].

We hypothesized that the previously characterized paracrine and immunomodulatory properties of HUCPVC would be the key in mediating either pro- or antigrowth effects on tumor cells. Here, we investigated the effects of HUCPVC on breast cancer and melanoma cell growth using an *in vivo* xenograft human melanoma tumor-bearing mouse model and *in vitro* assays using five independent cancer cell lines as a first step to assess the safety and suitability of HUCPVC treatment in preventing the side effects of chemotherapy in oncological patients.

2. Materials and Methods

2.1. Cell Culture. Previously established and extensively characterized lines of FTM and term HUCPVC [8, 17–20] (Figure S1) and human fibroblasts (HS-68, ATCC) were expanded in Alpha-Modified Minimum Essential Medium (αMEM) (Hyclone), with 2.5% human platelet lysate (HPL) good manufacturing practice grade plus cell culture supplement (Compass Biomedical) and 1% penicillin and streptomycin (Gibco). Human melanoma cells (SK-Mel-28, A375, ATCC), and three breast cancer cells (SK-BR-3, ATCC, and HTB-30), (MCF7, ATCC, and HTB-22), and (MDA-MB-231, ATCC, and HTB-26) were expanded in a similar fashion using ATCC-Formulated Eagle's Essential Medium, supplemented with 10% fetal bovine serum (FBS) (Hyclone) and 1% penicillin and streptomycin. Cell passaging was performed using TrypLE (ThermoFisher Scientific) at 37°C for 5 min. Resuspended live cells were counted using an automated cytometer and trypan blue exclusion and were plated at densities of 4,000 cells per square centimeter (2×10^5–2.5×10^5 cells in a 10 cm^2 plate). Cell cultures were maintained at 37°C and 5% CO_2.

2.2. Human Melanoma Tumor-Bearing Xenograft Mouse Model and Tumor Growth Assessment. Cells used in this study were confirmed to be rodent and human pathogen-free (IDEXX Bio Analytics, IMPACT I and h-IMPACT I). 5×10^6 SK-Mel-28 cells were resuspended in 75 μL phosphate buffered saline (PBS) and mixed with 25 μL of Matrigel (Corning). 6–8-week-old Nonobese diabetic/severe combined immunodeficiency (NOD

SCID) mice (Charles River) were anesthetized with 5% isoflurane and maintained at 2.5% while the cell mixture was injected subcutaneously. When tumors were palpable (around 10 days after SK-MEL-28 injection), animals were randomized to four groups ($n = 15$ animals per group) using an online randomization software (randomisation.com). 1×10^6 HUCPVC from three independent lines (FTM 1, FTM 2, and term) were suspended in $200 \mu L$ Hank's balanced salt solution (HBSS) and injected intravenously via the tail vein by a blinded technician. Controls were injected with HBSS (Life Technologies). A subset of these animals ($n = 6$ per group) received HUCPVC prelabeled with Qtracker 625 fluorescence (ThermoFisher Scientific) according to the manufacturer's instructions. Animal weights were recorded on Day 0 and on the end point day. Tumor size ($n = 12$ per treatment) was measured weekly over a span of three weeks following HUCPVC injection using a digital Traceable Carbon Fiber Caliper (VWR). Tumor volume in mm^3 was calculated using the formula: Volume $=$ (width)$^2 \times$ length/2. Animal health was monitored daily. Mice were anesthetized at 24 hr ($n = 3$ per group) or 3 weeks ($n = 12$) with 5% isoflurane and sacrificed by transcardial perfusion. The mice were perfused with 20 mL of cold PBS, then 20 mL of cold 4% paraformaldehyde (PFA, ThermoFisher Scientific). The tumor, spleen, lungs, and liver were dissected and transferred in 4% PFA at 4°C overnight. Tissues were transferred to 30% sucrose at 4°C overnight and embedded with OCT (The Cryo-embedding compound, Electron Microscopy Science) on to Fisherbrand disposable base molds ($24 \times 24 \times 5$ mm) and stored at −80°C.

2.3. Cell Tracking, Immunostaining, and Fluorescence Microscopy.

10-μm-thick nonconsecutive frozen sections encompassing the entire tumor, lung, and liver tissue were collected on Tru Scientific adhesive microscope slides (Tru-Bond 380, MATSUNAMI) using a Leica CM1900 cryostat. Slides were stored at −80°C. Prior to immunostaining, slides were washed in PBS, incubated in 4% PFA for 10 min, and then washed three times in PBS. A blocking solution (PBS, 10% normal goat serum, 1% BSA, and 0.3% Triton X) was added to the slides for 1 hr at room temperature (RT). After blocking, the sections were incubated with primary antibodies for 1 hr at RT or overnight in a humidified chamber at 4°C. The primary antibodies used were: rabbit antis-CD68 (1 : 100, Abcam, ab125212), rabbit anti-Ki67 (1 : 500, Abcam, ab15580), anti-IsolectinB4 biotin-XX conjugate (1 : 500, ThermoFisher Scientific, 121414), mouse anti-MMR/CD206 (1 : 500, R&D systems, AF2535), and rabbit antihuman cleaved caspase-3 (1 : 500, Abcam, AB13847). Secondary antibodies used included goat antirabbit Alexa Fluor488 (1 : 1000, ThermoFisher, A11034), Donkey Anti-Goat IgG H&L, and AlexaFluor 488 (1 : 1000, ThermoFisher, A11055). Subsequently, the sections were incubated with corresponding fluorescent-labeled secondary antibodies diluted in half concentrated block solution and added for 90 min in a humidified chamber at 4°C. Sections were counterstained with Hoechst 33,342 solution (1 : 1000, ThermoFisher Scientific) for 3 min. The slides were washed three times in PBS, kept in mounting media (PermaFluor, Thermo-Fisher Scientific), sealed with glass coverslips and imaged using the EVOS FL auto 2 imaging system (Life Technologies). Eight representative images were taken of each tissue section. For tumor assessments, four random images of the tumor core and four of the periphery were taken on each section. The number of positive signals was quantified using the ImageJ ITCN Image processing and analysis in Java. Qdot imaging was performed on the same day as immunostaining to obtain high-quality brightness and detection for images. All tumors were imaged and quantified by an observer blinded to treatment groups. For manual counting of Hoechst-stained nuclei, images were divided into either two or four representative sections and the cells were subsequently counted. The total number of cells per image was obtained by multiplying the number of cells per half or quarter image by 2 or 4, respectively. Manual counting was performed for CC3, CD206, and CD68 analyses. For IB4 and Ki67, the number of positive signals was quantified using the ImageJ ITCN, Image-based Tool for threshold function/area covered.

2.4. Flow Cytometric Analysis of Immune Cells in Tumors.

A tumor xenograft study was performed including three groups treated with FTM 2, fibroblast (FIBS) or HBSS control ($n = 5$). Tumors were harvested and weighed at 3-weeks postcell injection and transferred on ice and minced into 1–2 mm pieces and digested in 5 mL of RPMI (Gibco), containing 1 mg/mL Collagenase//Hyaluronidase (Sigma Aldrich), 4 mg/mL of trypsin-EDTA 0.05% Trypsin/EDTA 4 NA (Life technologies), and 1 mg/mL DNase I (Stemcell technologies). After incubation of 2 hr at 37°C, the digested tumor tissue was filtered with a 70 μm nylon filter (Fisherbrand) to obtain a single-cell suspension. Cells were counted using an automated cell counter (Eve, automatic cell counter, NanoEntek) and 50,000 cells were prepared in 200 μL of 3% FBS–PBS solution per reaction. 5 μL of fluorophore-conjugated antibodies and viability dyes (all from Miltenyi Biotech) were added, mixed properly and incubated for 20 min at 4°C. Flow cytometry was performed using MACSQuant Analyzer 10 multicolor digital flow cytometry (Miltenyi Biotech). FlowJo™ software was used for flow data analysis. Two reaction sets were prepared which included: Cell Tracer Green (CMFDA, Thermo Fisher Scientific), Vioblue-conjugated antimouse CD45 antibody, APC-conjugated antimouse NK 1.1 antibody, 7-aminoactinomycin D (7-AAD), Viogreen-conjugated mouse anti-CD45, PEVio770-conjugated antimouse CD11b, Vioblue-conjugated antimouse LY6G, A, and PE-conjugated antimouse LY6C PE. CD45 +ve cells were selected from live cells gated from the total cell population (Cell Tracer green+) and the NK1.1 +ve population (putative NK cells) was selected within the CD45 +ve population. Alternatively, dead cells were excluded using 7AAD. CD45+ cell was selected from live cells, and the CD11b +ve population within it. Putative monocytes were characterized as CD45+, CD11b+, Ly6C +, and Ly6G−, whereas neutrophils were characterized as CD45+, CD11b+, Ly6C−, and LY6G+.

2.5. Blood Collection and Enzyme-Linked Immunosorbent Assay (ELISA).

Mouse serum was isolated from blood collected into collection tubes (BD vacutainer, BD) from the lateral saphenous vein once a week from each animal

($n = 5$) for 3 weeks, starting on the tumor xenograft injection day. Cardiocentesis was performed at the 3-week endpoint in a terminal procedure to obtain a larger volume. Blood samples were allowed to clot for 2 hr at RT before centrifuging for 20 min at 2,000 g. Serum was transferred to new tubes and stored at −80°C until assayed. 50 μL mouse serum (undiluted) for TNF-α and 10 μL mouse serum diluted 1 : 2000 for C-reactive protein (CRP) assays were used in duplicate wells. Mouse TNF-α and CRP concentrations were measured in serum samples using the Quantikine HS Elisa Kit (R&D Systems), as per the manufacturer's instructions. The plates were read with a plate reader (FilterMax F5, Molecular Devices) at 450 nM. TNF-α and CRP concentrations were calculated for each sample using the standard curve.

2.6. In Vitro Coculture of HUCPVC with Human Melanoma and Breast Cancer Cell Lines. Cancer cells were plated in 12-well plates at a density of 15,000 cells per well in 1 mL media. The same HUCPVC lines (20,000 cells) and fibroblasts (to control for nonspecific cellular effects) used in the *in vivo* experiments as well as additional HUCPVC lines were seeded in 0.4 μm Transwell™ inserts (Corning) containing 500 μL of alpha-MEM with 2.5% HPL and 1% pen-strep. The inserts were incubated overnight in 5% CO_2 at 37°C in 12-well plates containing 1 mL of αMEM with 2.5% HPL and 1% pen-strep. After incubation, the inserts were transferred to 12-well plates containing cancer cells. The cocultures were incubated for 72 hr. All cell combinations and controls were grown in triplicate wells.

2.7. Assessment of Cell Viability and Growth in Coculture Assays. The number of live cells was measured using the Cell Counting Kit-8 (CCK-8, Sigma Aldrich), as per manufacturer's instructions. Cell counting solution was added to cell cultures at one-tenth the volume of media and live cell numbers were determined by measuring the optical density at 450 nm (OD450). Using flow cytometry, a standard curve at OD450 as a function of live cell number was generated to confirm the linearity of this assay (Figure S2).

2.8. Colorimetric Lactate Dehydrogenase (LDH) Assay. Media was harvested from cocultures, centrifuged to remove cell debris and stored at −20°C. On the day of the assay, reagents from the Cytotoxicity Detection Kit (Roche) were prepared, according to the manufacturer's protocol. Samples were thawed and centrifuged at 3,000 rpm for 5 min. A 100 μL of supernatant was transferred to the assay plate. 100 μL of the mixed detection kit reagent was then added to each of the assay wells on top of the supernatant in rapid succession. The total volume in each well was 200 μL. The assay plates were then incubated at RT in the dark for 30 min. Colorimetric LDH measurements were quantified with a plate reader (FilterMax F5, Molecular Devices) at 490 nm, as we described previously [16, 18].

2.9. RNA Extraction, cDNA Conversion, and qPCR. RNA was extracted from cancer cells (12-well plates) using the Norgen Total RNA Purification kit (Norgen Biotek), according to the manufacturer's instructions. Briefly, buffer RL + 1% b-mercaptoethanol (v/v) were added to the cell pellet and lysed by repeatedly passing the suspension through a 25G needle.

RNA from this lysate bound to the column and impurities were washed away. The eluted RNA was quantified using the Qubit RNA high-sensitivity assay (ThermoFisher Scientific). 200 ng of RNA was reverse transcribed using SuperScript VILO IV (ThermoFisher Scientific) with DNase digestion, according to the manufacturer's instructions. The resulting cDNA was used for qPCR. Gene expression of *CCND1* and *TP53* was assessed using predesigned and validated PrimeTime™ qPCR assays (IDT) with *GAPDH* as the reference gene. All targets were assayed in duplicate using PrimeTime™ gene expression masterMix (IDT) (polymerase activation at 95°C for 3 min; 45 cycles of 15 s denaturation at 95°C and 1 min annealing/extension at 60°C). Relative fold change ($\Delta\Delta$Ct) was employed to quantify gene expression. The list of primers and probes used for qPCR are given in Table S1.

2.10. Statistical Analysis. All *in vitro* results were generated from at least three independent experiments using at least three independent FTM HUCPVC lines and three term HUCPVC lines. Histological analysis results were generated from the mean values of 4–8 images for each tissue slide, as indicated in the figure legends. Results were presented as mean ± standard deviation, unless otherwise indicated in figure legends. Statistical analyses were conducted using GraphPad Prism 9.1.0 (GraphPad Software). Intergroup comparisons were assessed using one-way analysis of variance (ANOVA). If significant, post hoc Tukey multiple comparisons tests were conducted to specify differences between experimental groups. Significant differences were delineated as follows: $^*p < 0.05$, $^{**}p < 0.01$, $^{***}p < 0.001$, $^{****}p < 0.0001$.

3. Results

3.1. Systemic Administration of HUCPVC in a Melanoma Tumor-Bearing Model Leads to a Reduction in Tumor Tissue Size. There were no significant differences in mean tumor volumes between animal groups treated with FTM 1, FTM 2, and term HUCPVC and HBSS controls on Day 0 ($P > 0.8$) (Figure 1(a)). Tumor volume for animals treated with HBSS increased significantly over 3 weeks relative to Day 0 ($P = 0.006$) (Figure 1(b)). Tumor volumes in animal groups treated with one line of FTM HUCPVC (FTM 2) and term HUCPVC decreased significantly at 3 weeks compared to Day 0 ($P = 0.004$, $P = 0.04$, respectively) (Figure 1(b)) and were significantly reduced compared to the control group at this time point ($P < 0.0001$) (Figure 1(a)). Tumor volumes significantly increased in animals treated with a second FTM line (FTM 1) ($P = 0.0078$) (Figure 2(b)) and were not significantly different from HBSS controls in this group ($P > 0.9999$) (Figure 1(a)). After dissection at 3 weeks, it was apparent that tumor size was decreased in all cell-treated groups (Figure 1(c)) and tumor weights were reduced by 2.3-fold to fourfold ($P < 0.05$) in all cell-treated groups compared to the control group (Figure 1(d)).

3.2. HUCPVC Treatment Leads to a Reduction in Proliferating Tumor Cells but No Significant Changes in Tumor Cell Apoptosis or Vascularization. To further understand the cellular mechanisms for the observed tumor size reduction,
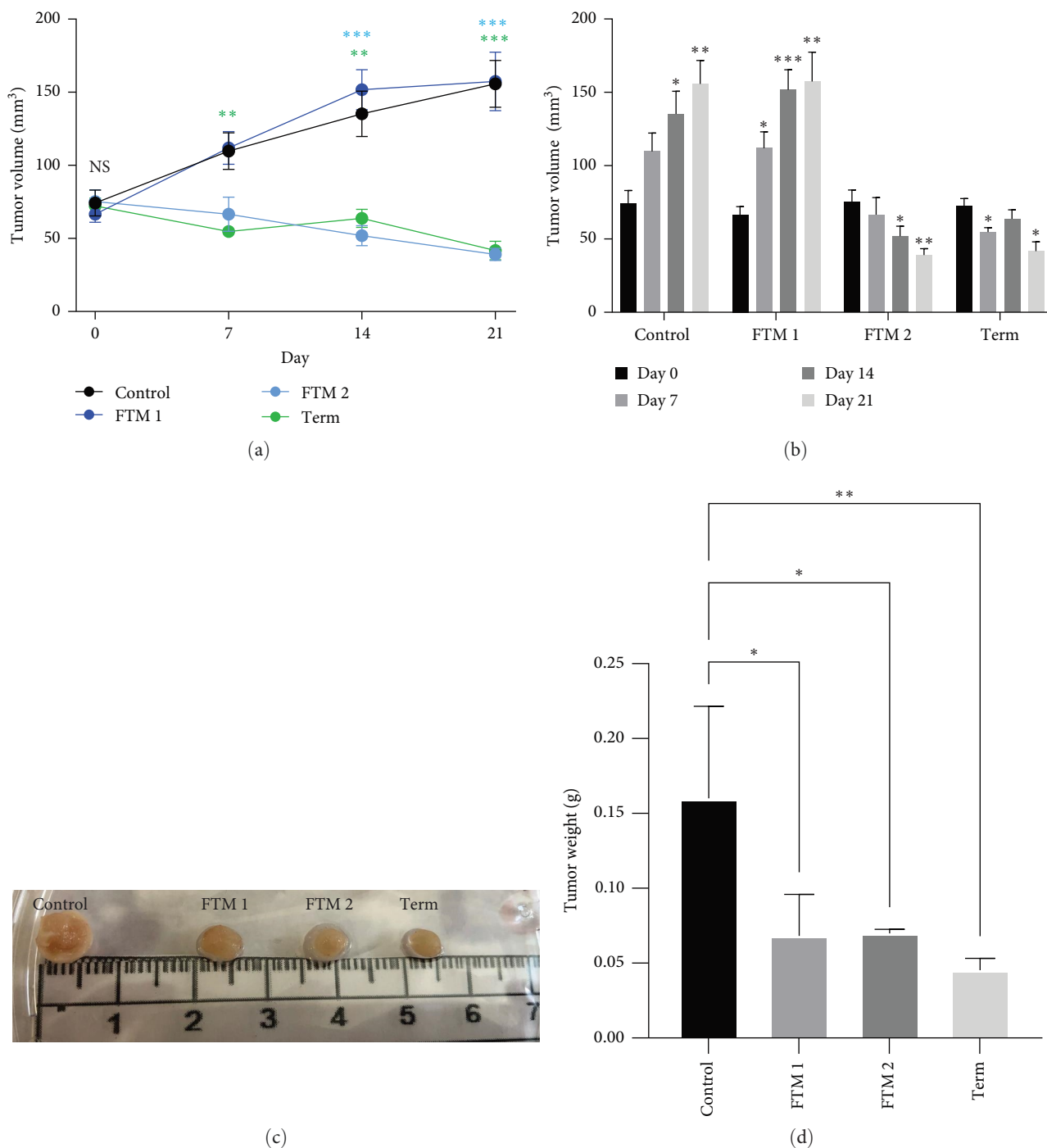
(a)

(b)

(c)

(d)

FIGURE 1: Tumor growth in a human SK-MEL-28 tumor-bearing xenograft mouse model. Calculated tumor volume over 21 days in the SK-MEL-28 tumor xenograft NOD SCID mouse model treated with three lines of HUCPVC (FTM 1, FTM 2, and term) or HBSS (control), $n = 11$–12 per group. Three independent experiments were performed and animals were randomized on Day 0. Measurements were done by a blinded observer. (a) Time course showing FTM 2 and term HUCPVC-treated animals have significantly reduced tumor volume when compared to controls (and FTM 1) at Day 7, 14, and 21. FTM 1-treated animal tumors do not significantly differ from controls (and FTM 2 and Term 1 do not significantly differ from each other). Error bars represent SEM. (b) Weekly tumor volume plotted by group, showing statistically significant differences between Day 0 and other timepoints for each study group. (c) Images of representative tumors after dissection at 3 weeks. (d) Tumor weights after dissection at 3 weeks ($n = 4$ per group). Error bars represent SEM *, $P < 0.05$; **, $P < 0.01$, ***, $P < 0.001$.
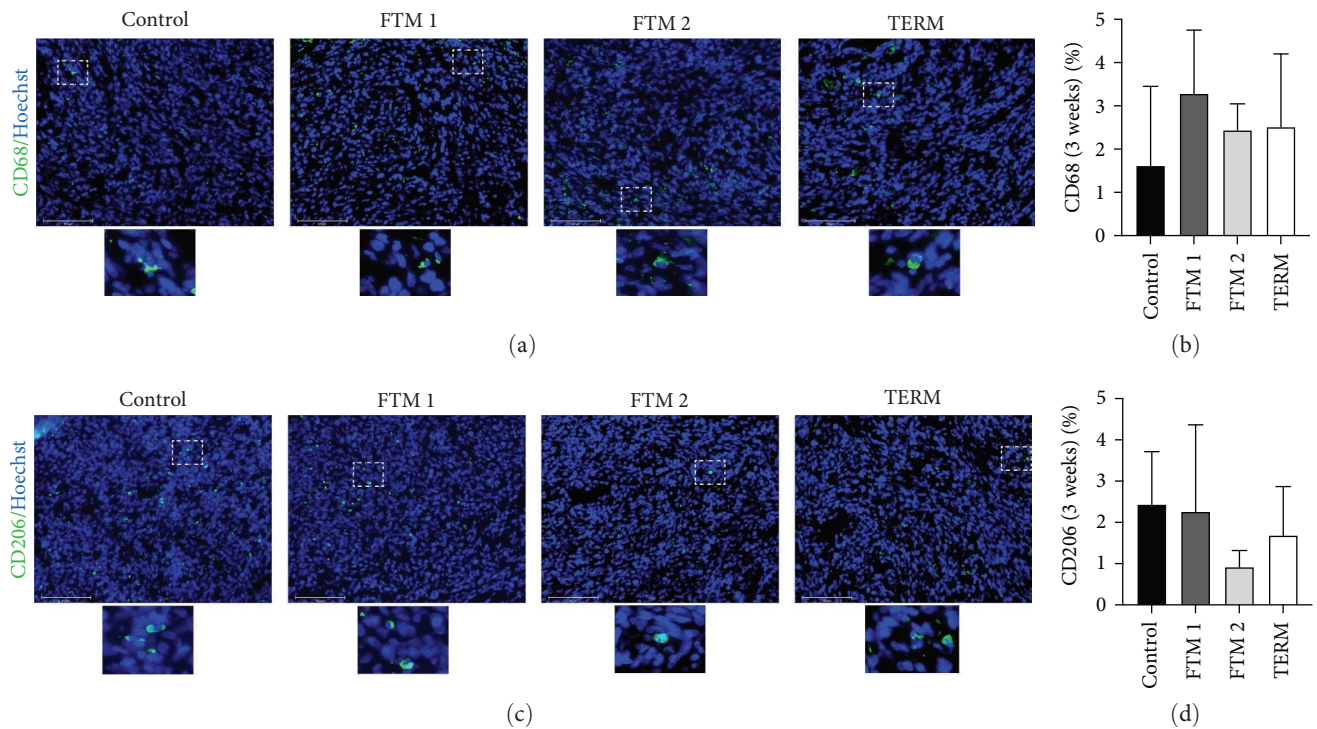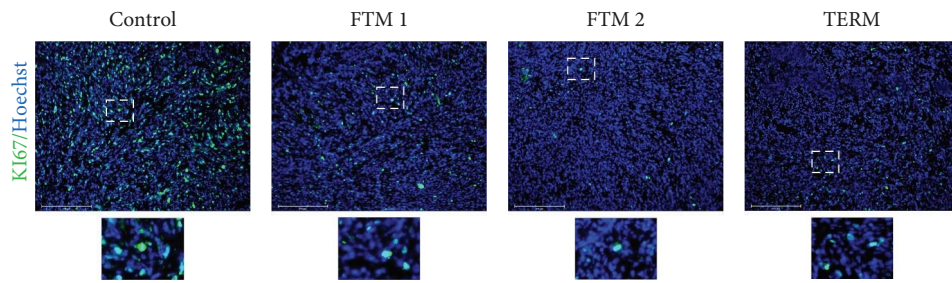
(a)

(b)

(c)

(d)

FIGURE 2: Analysis of macrophage subpopulations in SK-MEL-28 tumors of xenograft mouse model treated with HUCPVC. (a–d) Representative immunostaining images of SK-MEL-28 tumor xenograft NOD SCID mouse model three weeks after animals were treated with two FTMs (FTM 1 and FTM 2), one term HUCPVC lines or HBSS as a control and quantification for the proportion of (a and b) CD68+ cells (pan-macrophage marker, sometimes associated with type 1 macrophages), (c and d) CD206+ cells (type 2 macrophage marker). Error bars represent SEM. No significant differences were observed between the groups. Scale bar = 125 μm. $n = 4, 3, 4$, and 4 for control, FTM 1, FTM 2, and TERM, respectively. Insets represent twofold magnification.

tumor tissue sections were immunostained for Ki67 (proliferating cells), cleaved caspase-3 (apoptotic cells) and isolectin B4 (endothelial cells). The proportion of Ki67+ cells within the tumor at 3 weeks decreased by 2-fold to 2.5-fold in all cell-treated groups compared to the control group ($P = 0.002$, $P = 0.004$, and $P < 0.01$, respectively) (Figures 3(a) and 3(b)). The proportion of cleaved caspase-3 positive cells was not altered in the tumor tissue of HUCPVC-treated animals when compared to controls at 3 weeks following injection ($P = 0.96$). Less than 0.5% of all cells (labeled with Hoechst) were positive for human cleaved caspase-3 (Figures 3(c) and 3(d)). The proportion of surface area covered by isolectin B4 staining was also not significantly altered in the HUCPVC treatment groups when compared to controls ($P = 0.66$) (Figures 3(e) and 3(f)).

3.3. HUCPVC Do Not Alter the Proportion of Immune Cells in the Tumors but May Modulate Inflammatory Status. At 3 weeks, there were no significant changes in the proportion of tumor cells expressing the pan-macrophage marker CD68 in the control group or HUCPVC-treated animals (Figures 2(a) and 2(b)). Additionally, no significant changes were found for the M2 macrophage-associated marker CD206 in the tumor tissue of controls or HUCPVC-treated animals (Figures 2(c) and 2(d)).

To further assess immune cell populations in tumor tissue, the tumor growth study was repeated with three groups:

HBSS control, FTM 2, and fibroblast cells (FIBS). As in previous experiments, the systemic delivery of FTM 2 led to a significant reduction in tumor volume within 7 days of treatment ($P < 0.01$), and every subsequent week ($P < 0.001$). In contrast, tumor volume in the control group increased significantly after week 2 ($P < 0.05$) and week 3, when compared to Day 0 ($P < 0.0001$). FIBS treatment led to a significant increase in tumor growth by week 3 when compared to Day 0 ($P < 0.01$), but was significantly reduced when compared to that of the control group at that timepoint ($P < 0.05$) (Figure 4(a)). Tumor weight at 3 weeks was significantly reduced in the FTM 2 group, when compared to the control and FIBS groups ($P < 0.01$ and 0.05, respectively) (Figure 4(b)). The proportion of viable cells measured by 7AAD exclusion and flow cytometry was not different between the groups (Figure 4(c), Figure S3). There were neither statistically significant differences in the proportion of leukocytes (CD45+) (Figure 4(d)) nor in the proportion of putative NK cells (NK1.1+SSC low) (Figure 4(e)), monocytes (CD11b+, Ly6C+, and Ly6G−) (Figure 4(f)) or neutrophils (CD11b+, Ly6C−, and Ly6G+) (Figure 4(g)) between the three groups (Figure S3). Serum levels of the proinflammatory cytokine, TNF-α, were significantly reduced in the FTM 2-treated animals, when compared to HBSS ($P < 0.0001$) and FIBS ($P < 0.001$) controls at week 2 and week 3 (Figure 4(h)). In comparison to prestudy levels, serum CRP levels were found to be significantly increased in control ($P < 0.01$) and FIBS ($P < 0.001$) groups at 3 weeks, but were not significantly
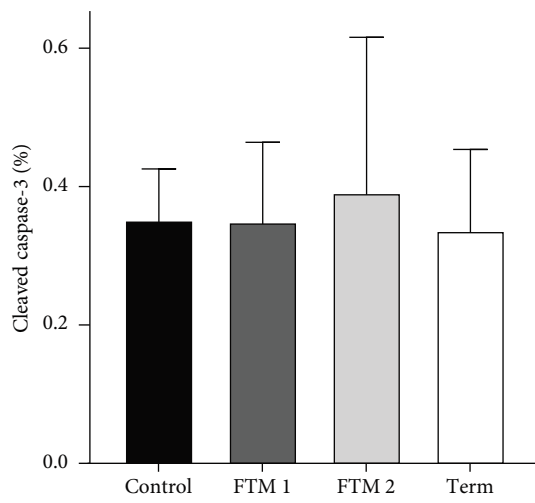
(a)
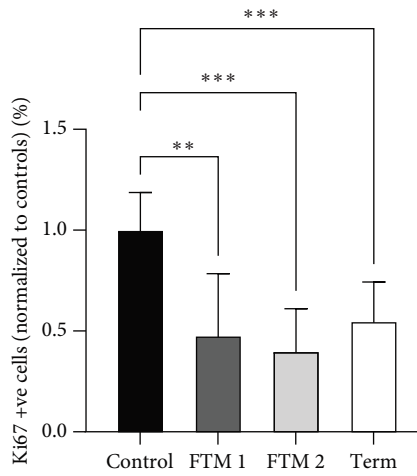
(b)
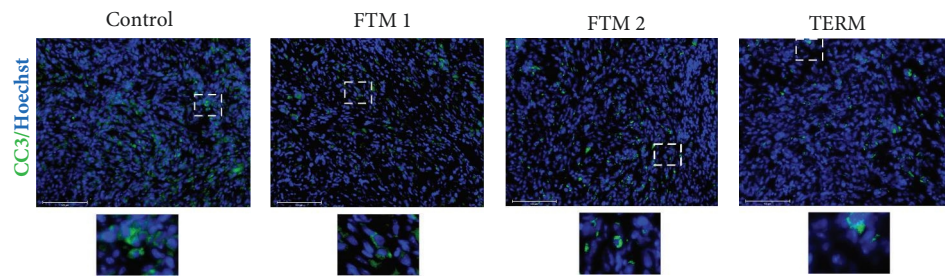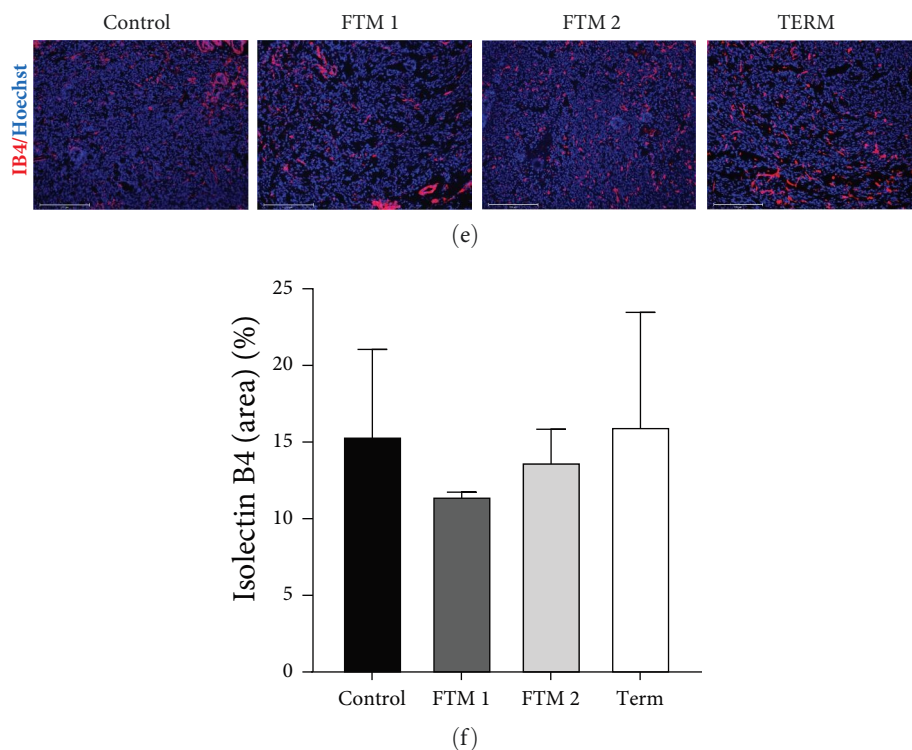

(c)

(d)

FIGURE 3: Continued.

(e)

(f)

FIGURE 3: Analysis of cell proliferation, apoptosis, and vascularization in SK-MEL-28 tumors of xenograft mouse model treated with HUCPVC. (a–f) Representative immunostaining images of SK-MEL-28 tumor xenograft NOD SCID mouse model three weeks after animals were treated with two FTMs (FTM 1 and FTM 2), one term HUCPVC lines or HBSS as a control. Quantification and proportion of (a and b) Ki67+ cells (scale bar = 125 μm), (c and d) cleaved caspase-3+ cells (CC3, scale bar = 275 μm), and (e and f) isolectin B4+ cells (IB4, scale bar = 275 μm) were measured to assess proliferation, apoptosis, and vascularization, respectively. Error bars represent SEM **, $P < 0.01$, ***, $P < 0.001$. Insets represent twofold magnification.

increased in FTM 2-treated animals at this timepoint ($P = 0.8$). CRP levels were significantly decreased in the FTM 2-treated animals when compared to control ($P < 0.05$) and FIBS ($P < 0.01$) (Figure 4(i)) groups.

3.4. Qdot-lLabeled HUCPVC Localize Mainly to Lungs and Liver, and Very Few Localized to Tumors. To assess the biodistribution of HUCPVC injected in a NOD SCID tumor-bearing model, we quantified the QTracker signal in the lung, liver, and tumor of dissected animals isolated 24 hr following injection. We found that very few qdot signals were present in the tumor (representing 0.00%–0.03% of total cells) (Figures 5(a) and 5(b)) and that they were more abundant in the lungs (representing 0.3%–1% of total cells, for FTM 1, FTM 2, and term, respectively) (Figures 5(c) and 5(d)) and liver (representing 0.7%–2% of total cells, respectively) (Figures 5(e) and 5(f)) at 24 hr. We performed qdot labeling and analyzed tumor tissue after 3 weeks. While the proportion of tumor cells labeled with qdot was low, we found an increased proportion of Hoechst +ve cells that colocalized with qdots in the FTM 1 group ($0.29\% \pm 0.15\%$) when compared to FTM 2 ($0.11\% \pm 0.06\%$) and term ($0.12\% \pm 0.04\%$) at this time point ($P < 0.05$) (Figures 5(g) and 5(h)).

3.5. A Large Proportion of Qdot Labeled-HUCPVC Colocalize with Macrophage Markers in the Liver and Lung, but Not in Tumors. The colocalization of QTracker-label with CD68, a pan-macrophage marker, was quantified in the liver, lungs,

and tumor to assess the proportion of HUCPVC that may be phagocytosed. We found that in the lungs, a proportion of Qdot-labeled HUCPVC colocalized with CD68 (representing 7%–14% of total cells) (Figures 6(a) and 6(b)). Higher proportions were observed in the liver as well (representing 25%–48% of total cells) (Figures 6(c) and 6(d)), but none of the qdots in the tumor colocalized with CD68 +ve cells 24 hr after injection into a NOD SCID mouse model. At 3 weeks, very few qdots colocalized with CD68 in the tumor (representing 1%–8% of total qdots, for FTM 1, FTM 2, term, respectively). Very few of the qdots colocalized with the M2 macrophage marker CD206 in the lung and tumor (Figure S4).

The proportion of CD68 +ve cells in the lung, liver, and tumor and CD206 +ve cells in the lungs were assessed at 24 hr to further examine a potential inflammatory response to HUCPVC treatment, and no significant differences were observed (Figure S5).

3.6. HUCPVC Alter Melanoma Cancer Cell Growth in a Cancer Cell-Line and HUCPVC Line-Dependent Manner Utilizing a Transwell™ Coculture Model. To further understand the effect of HUCPVC on melanoma cells, a Transwell™ coculture system and transendothelial invasion assays were used. At 72 hr, the fold changes of viable SK-Mel-28 cells exposed to independent lines of HUCPVCs or FIBS (cell control) in the coculture system were not significantly different from untreated controls (Figures 7(a) and 7(b)). At 72 hr, the fold
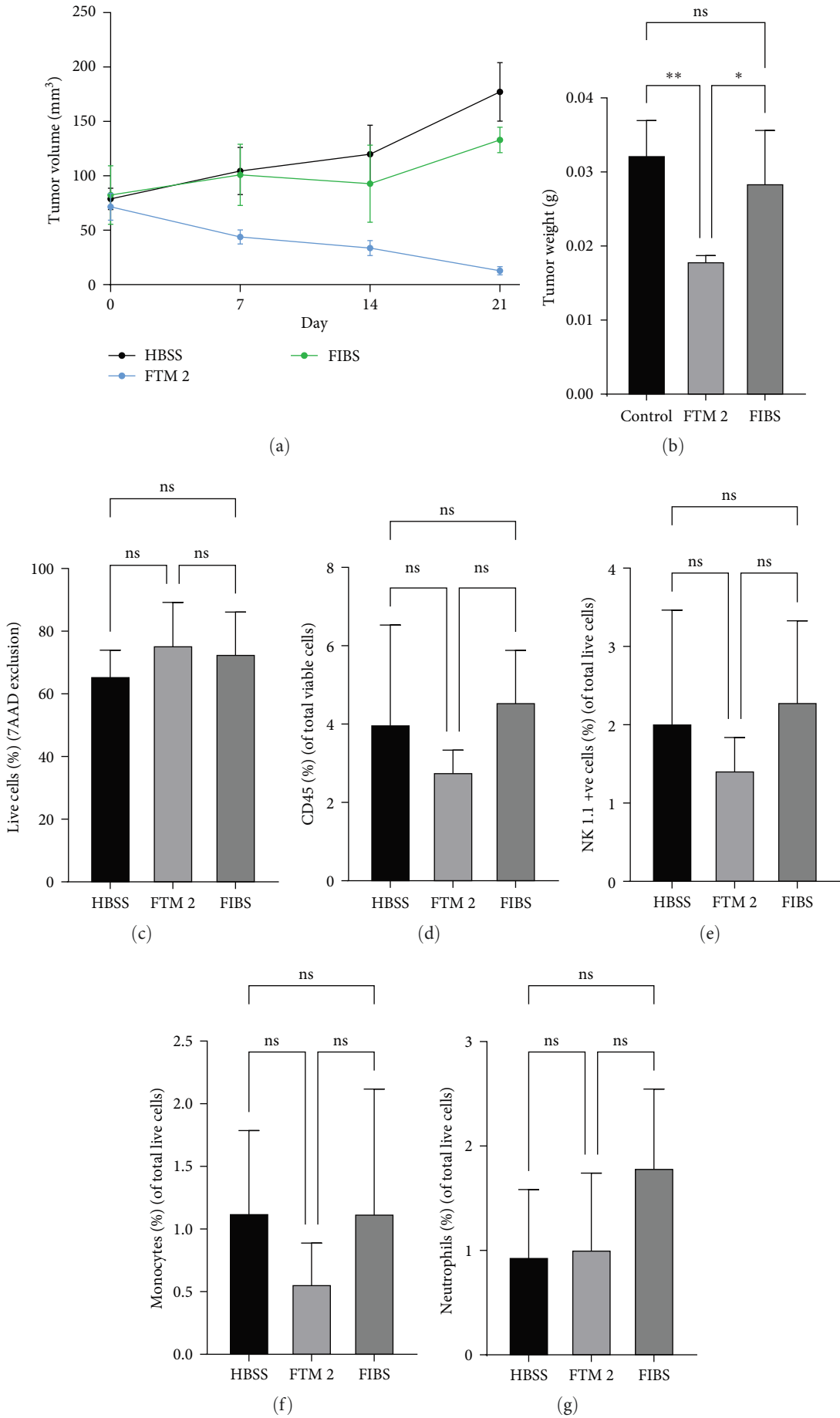
(a)

(b)

(c)

(d)
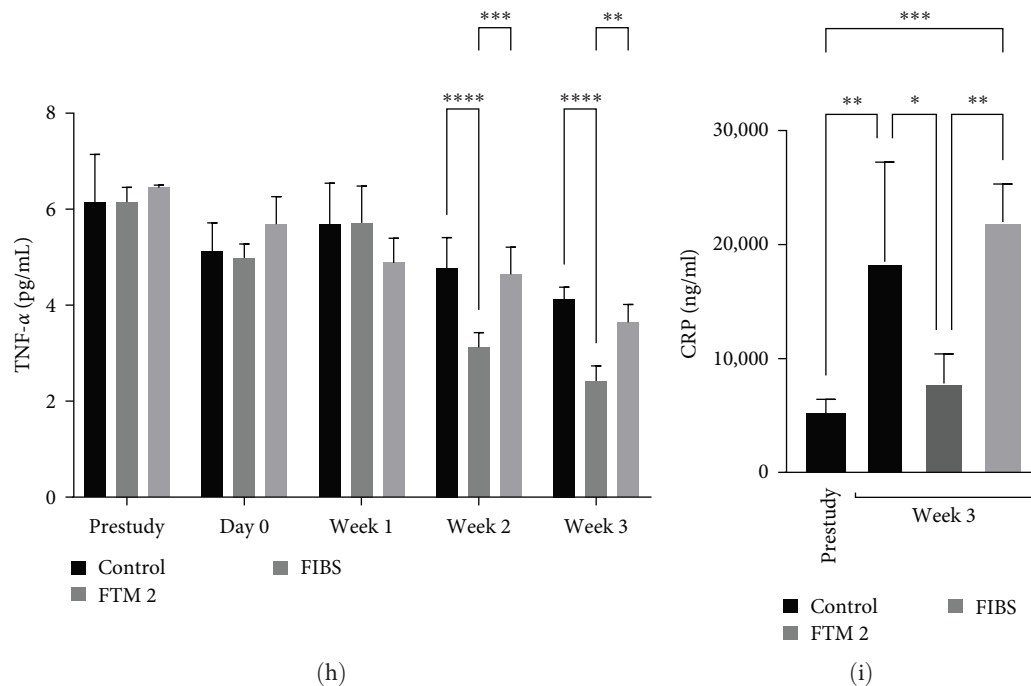
(e)

(f)

(g)

FIGURE 4: Continued.

(h)

(i)

FIGURE 4: Analysis of tumor growth, immune cells in the tumor, and serum levels of proinflammatory cytokine TNF-α and CRP, in a SK-MEL-28 tumor xenograft NOD SCID mouse model treated with FTM HUCPVC or fibroblasts. (a) Calculated tumor volume over 21 days in SK-MEL-28 tumor xenograft NOD SCID mouse model treated with one line of HUCPVC (FTM 2), fibroblast cells or HBSS (control), $n = 5$ per group. Animals were randomized on Day 0. Caliper measurements were done by the same blinded observer throughout the study. (b) tumor weights after dissection at 3 weeks. Error bars represent standard deviations *, $P < 0.05$; **, $P < 0.01$, ***, $P < 0.001$. (c–g) Flow cytometric analysis showing the proportion of live cells (c), CD45+cells (d), putative NK cell (e), monocyte (f), and neutrophil (g) subpopulations. (h) Serum TNF-α levels at 5 timepoints (prestudy, Day 0, Day 7, Day 14, and Day 21). (i) Serum CRP levels in animals prestudy ($n = 6$) and in controls, FTM 2- and FIBS-treated animals at 3 weeks. Error bars represent standard deviations *, $P < 0.05$; **, $P < 0.01$; ***, $P < 0.001$; ****, and $P < 0.0001$. $n = 5$ per group for all assessments.

change of A375 cells grown in coculture with FTM 1 and FTM 2 cells, but not four other lines, were significantly higher than controls (Figures 7(a) and 7(c); $p < 0.05$). No significant differences in LDH release were observed in SK-Mel-28 (Figure 7(d)) or A375 (Figure 7(e)) exposed to HUCPVC in coculture, when compared to untreated controls. SK-Mel-28 cells exhibited significantly increased invasion in coculture with FTM 3 cells, compared to controls (Figure 7(f); $p < 0.001$) but not with other cell lines. A375 cells demonstrated significantly decreased invasion in coculture with TERM 2 compared to controls (Figure 7(g); $p < 0.01$). but not with other cell lines. CCND1 expression in SK-Mel-28 cells was significantly increased after coculture with all term HUCPVC lines investigated (Figure 7(h); $p < 0.05$, $p < 0.01$, $p < 0.05$, but was less than twofold. No significant differences in SK-Mel-28 P53 expression were detected (Figure 7(i)). CCND1 and P53 expression in A375 cells were not altered in any of the coculture conditions (Figures 7(j) and 7(k)).

3.7. HUCPVC Alter Breast Cell Cancer Cell Growth in a Cell Line-Dependent Manner in a Transwell™ Coculture Model. The growth of MDA-MB-231 (Figures 8(a) and 8(b)) and SKBR3 (Figures 8(a) and 8(c)) cells were not significantly different after coculture with FTM and term HUCPVCs. At 72 hr, MCF7 cells in coculture with FTM 3 and TERM 1 cells exhibited significantly increased growth relative to

control cells (Figures 8(a) and 8(d); $p < 0.05$, $p < 0.05$). The addition of HUCPVC-conditioned media to breast cancer cells as an alternate model gave similar results (Figure S4). MDA-MB-231 invasion was significantly reduced by coculture with both TERM 1 and TERM 2 cells (Figure 8(e); $p < 0.05$, $p < 0.05$). No differences were observed in culture systems with FTM HUCPVC (Figure 8(e)). No significant differences in invasion were observed for SKBR3 (Figure 8(f)) and MCF7 (Figure 8(g)) cells after coculture with any FTM or term HUCPVC. CCND1 and P53 expression in MCF7 cells were not altered by coculture conditions Figures 8(h) and 8(i).

4. Discussion

Our data suggest that both FTM and term HUCPVC can inhibit melanoma tumor growth and even reduce the size of human melanoma tumors *in vivo*, in a SK-MEL-28 tumor-bearing immunocompromised mouse model. This effect appears to be specific to MSC, as fibroblasts injected in the same manner did not have an antitumor effect. *In vitro*, HUCPVC modulated cancer cell growth, viability, and invasion in a cancer- and HUCPVC-line dependent manner. To our knowledge, this is the first study to test the effect of MSC on cancer cell growth using multiple-independent donor-derived lines *in vitro* and *in vivo*.
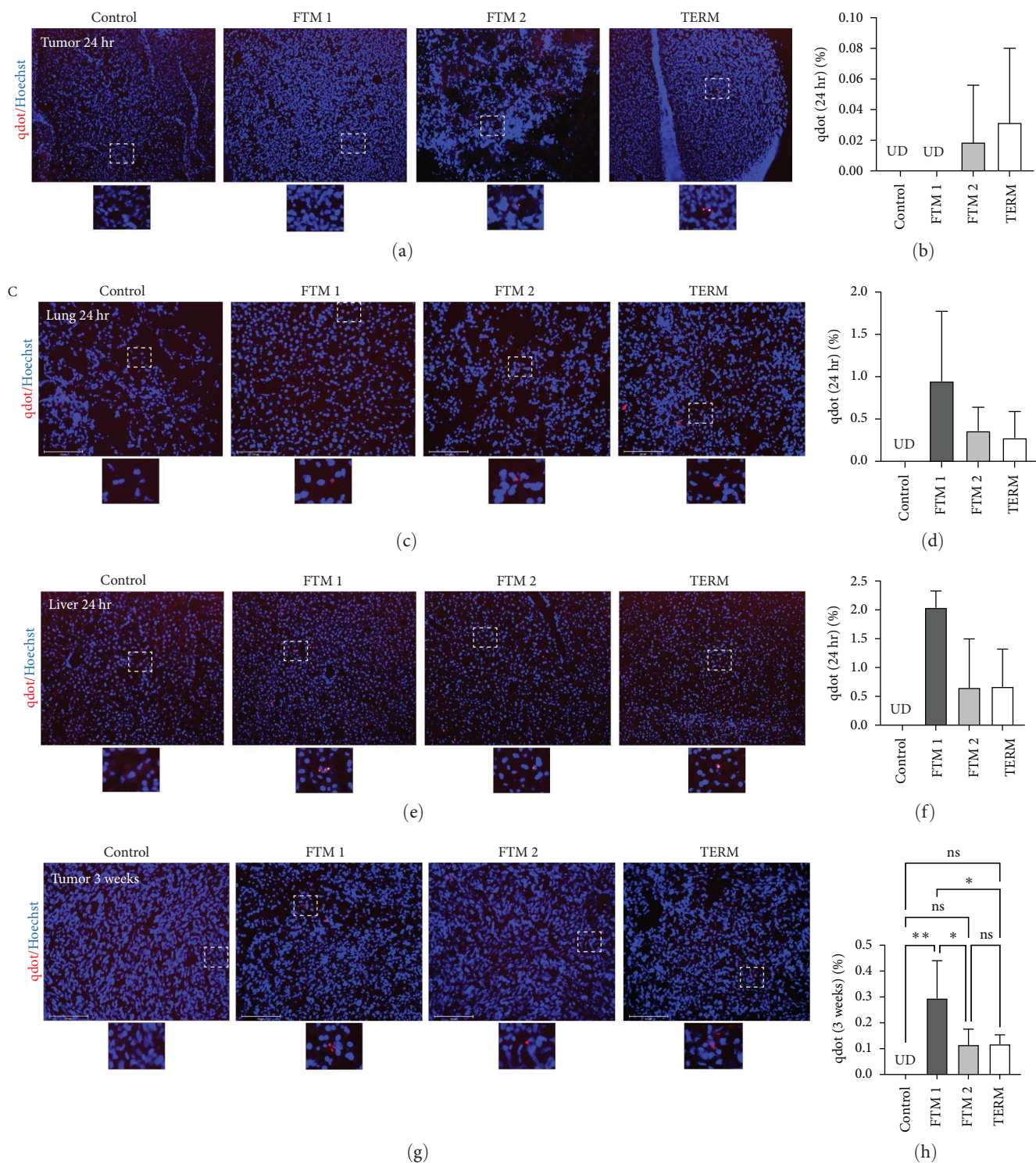
(a)

(b)

(c)

(d)

(e)

(f)

(g)

(h)

FIGURE 5: Quantification of qdot-labeling at 24 hr (tumor, lung, and liver) and 3 weeks (tumor) following systemic injection in the NOD SCID SKMEL28 xenograft model. (a–h) Representative immunostaining images of SK-MEL-28 tumor xenograft NOD SCID mouse model three weeks after animals were treated with two FTMs (FTM 1 and FTM 2), one term HUCPVC lines or HBSS as a control and quantification for the proportion of (a and b) CD68+ cells (pan macrophage marker, sometimes associated with type 1 macrophages), and (c and d) CD206+ cells (type 2 macrophage marker). Error bars represent SEM. No significant differences were observed between the groups. Scale bar = $125\,\mu$m. $n = 4$, 3, 4, and 4 for control, FTM 1, FTM 2, and TERM, respectively. Insets represent twofold magnification. $^{*}P < 0.05$; $^{**}P < 0.01$.

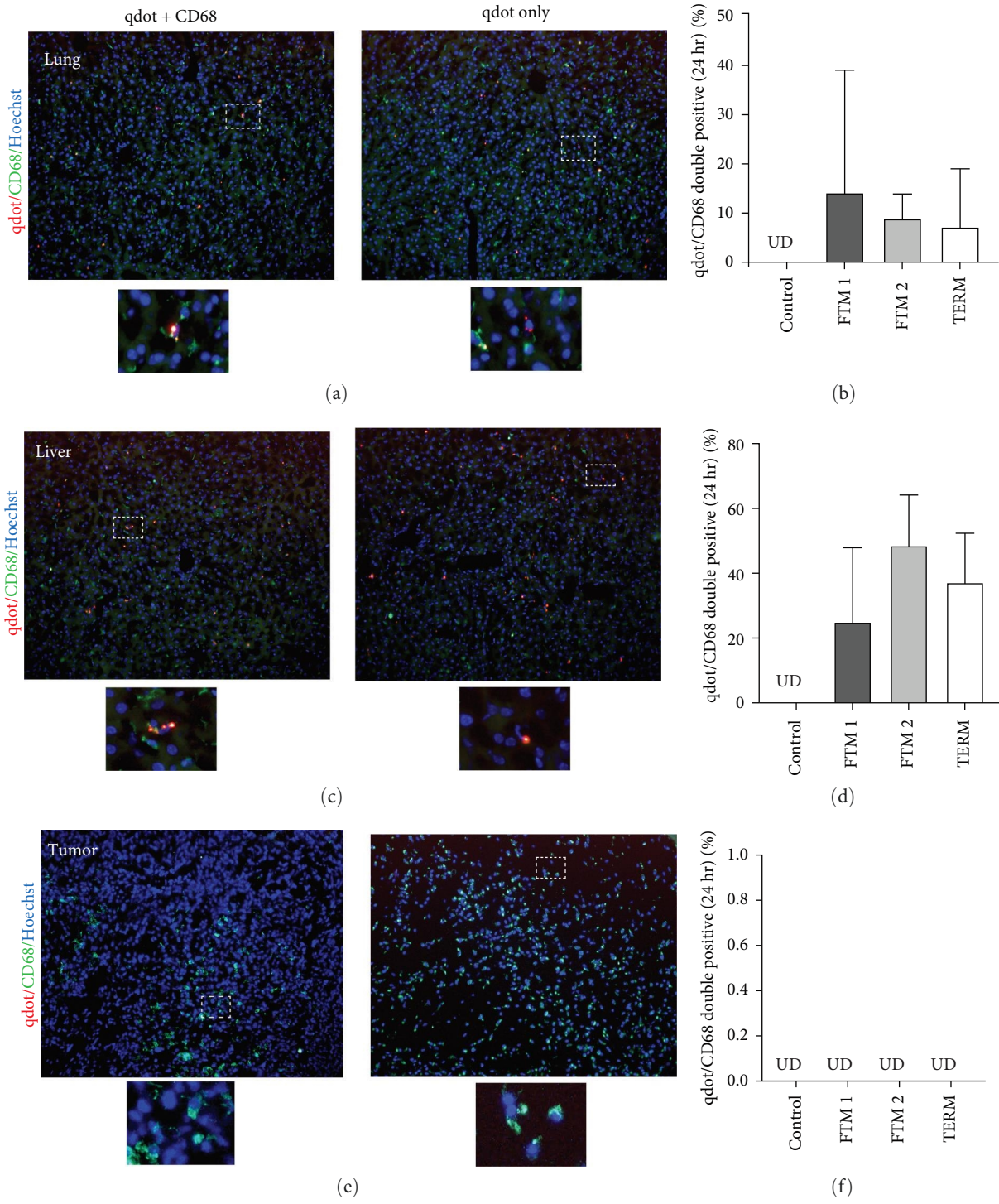(a)

(b)

(c)

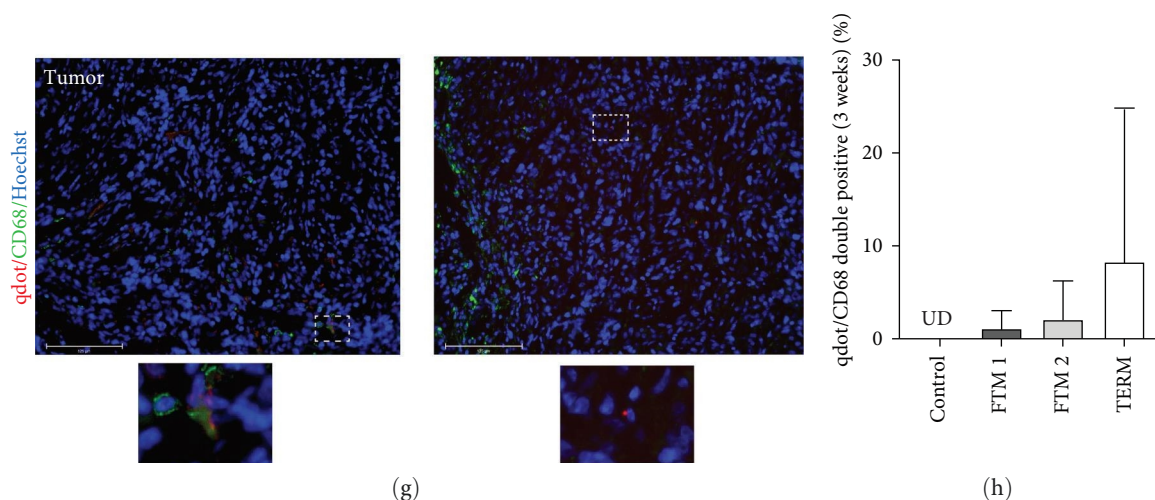(d)

(e)

(f)

FIGURE 6: Continued.

(g)

(h)

FIGURE 6: Quantification of qdot label colocalization with macrophage markers in the lung (24 hr), liver (24 hr), and tumor (at 24 hr and 3 weeks). Representative immunostaining images of SK-MEL-28 tumor xenograft NOD SCID mouse model 24 hr and three weeks after animals were treated with two FTMs (FTM 1 and FTM 2), one term HUCPVC lines or HBSS as a control and quantification for the proportion of (a and b) qdot localization in tumor tissue after 24 hr (c and d) qdot localization in lung tissue after 24 hr. (e and f) qdot localization in liver tissue after 24 hr. (g and h) qdot localization in tumor tissue after 3 weeks. Error bars represent SEM. No significant differences were observed between the 24-hour groups; however, significant differences were observed between the control and FTM 1, FTM 1 and FTM 2, and FTM 1 and TERM. Scale bar = 125 μm. Insets represent twofold magnification.

Overall, our results suggest that HUCPVC treatment may not only be safe as a cell therapy to prevent some of the side effects of cancer therapies in some cancer patients, but may also have antitumor effects. This is supported by comparisons of tumor growth and weight between treatment groups in the SK-MEL-28 tumor-bearing mouse model, where HUCPVC administration led to a significant decrease in tumor weight when compared to the control groups. Additionally, HUCPVC accumulated in the lung and liver and very few localized to tumors. This suggests that HUCPVC may modulate tumor growth through paracrine and/or immunomodulatory effects. It remains to be determined (1) whether the few persisting qdot labels observed in the tumor tissue sections at 3 weeks represent viable HUCPVC, as they could be remnants of phagocytosis or cell death that have accumulated in the tumor; and (2) what the implications of potentially viable cells are for long-term tumor growth. Qdot labels would not be expected to trace cells generated through HUCPVC proliferation, at least not beyond limited cell divisions, and as such other cell tracing approaches are warranted to confirm that viable HUCPVC have not migrated to tumors where they could have further paracrine effects on tumor growth.

Our *in vivo* data also suggest that treatment with HUCPVC leads to an overall reduction in tumor cell proliferation (Ki67) but no apparent changes in apoptosis (CC3), vascularization (IB4), innate system immune cells (CD45, NK1.1, and CD11b), including macrophage infiltration or polarization (CD68 and CD206) in the tumor tissue. TNF-α has been shown to be modulated by MSC treatment to reduce inflammation and regulate the immune response. A significant decrease in TNF-α was detected in the serum of FTM HUCPVC-treated animals, when compared to HBSS and fibroblast controls. TNF-α is a proinflammatory cytokine that has been associated not only with antitumor effects, but

also with promoting proliferation in melanoma cells [27]. It is possible that the reduced TNF-α levels or generally reduced inflammation contributed to the reduction in tumor growth. CRP is produced by hepatocytes in response to changes in IL-6 and IL-1 levels and generally thought to be an indicator of chronic inflammation. In the context of many cancers, it is a biomarker associated with tumor progression and poor prognosis [28–30], and recent studies suggest that high-CRP levels induce an immunosuppressive milieu in melanoma that favors tumor growth and metastasis [31]. In this study, the systemic delivery of FTM HUCPVC, but not a human fibroblast cell control, was shown to neutralize a tumor growth-associated increase in CRP levels. We have previously shown that HUCPVC administered intravenously can also decrease stress- or LPS- and age-induced CRP levels in immunocompetent animal models, and this response was not elicited to the same extent by human fibroblasts [8, 32, 33]. These results demonstrate a consistent immunomodulatory component of HUCPVC therapy, which may represent a key mechanism of their therapeutic effect.. Overall, this suggests that the stronger immunomodulatory properties of HUCPVC, compared to fibroblasts, may be associated with HUCVC-specific antitumor effects.

Our findings are, in part, consistent with the antitumor effects of other types of MSC observed in several other studies. Ahn et al. [12] noted a similar antitumor effect when human adipose tissue (AT)-MSC were repeatedly injected circumtumorally in an immunocompromised (BALB/c athymic) A375 melanoma tumor-bearing mouse model. Gene expression alteration of cell cycle components, as well as induction of apoptosis *in vivo*, were proposed as possible mechanisms for this observed effect. Although apoptosis might be one mechanism by which HUCPVC elicit their antitumor properties, we did not observe this in our *in vitro*
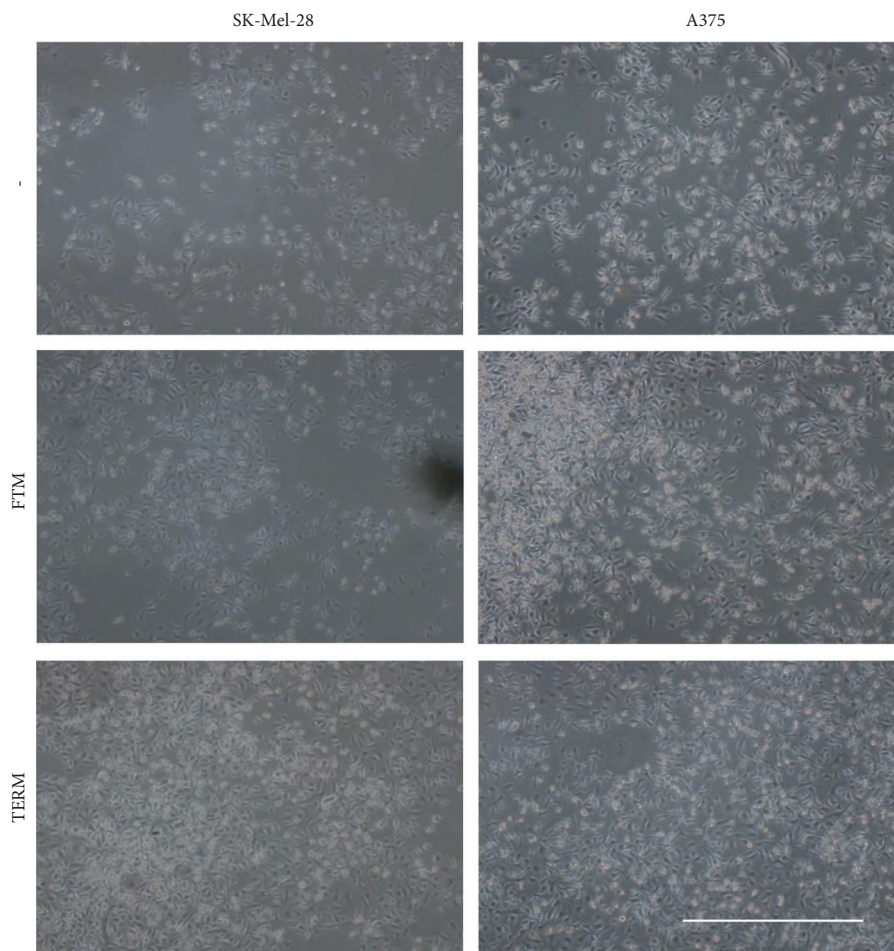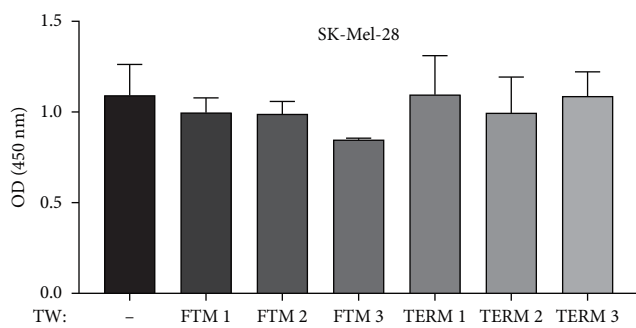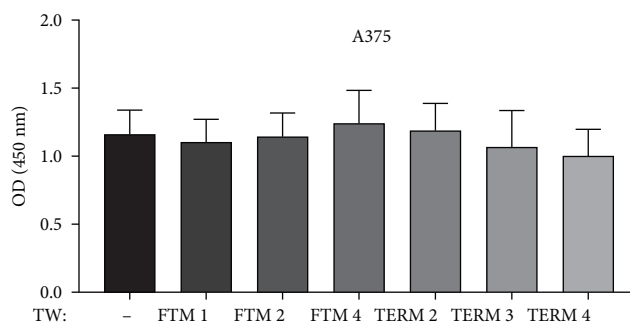
(a)
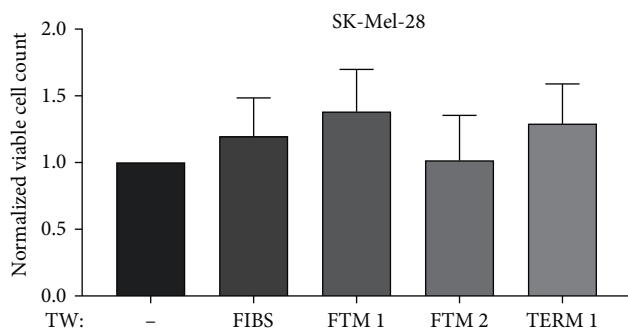
(b)
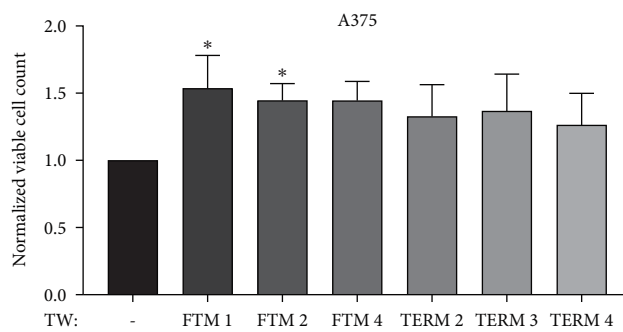
(c)
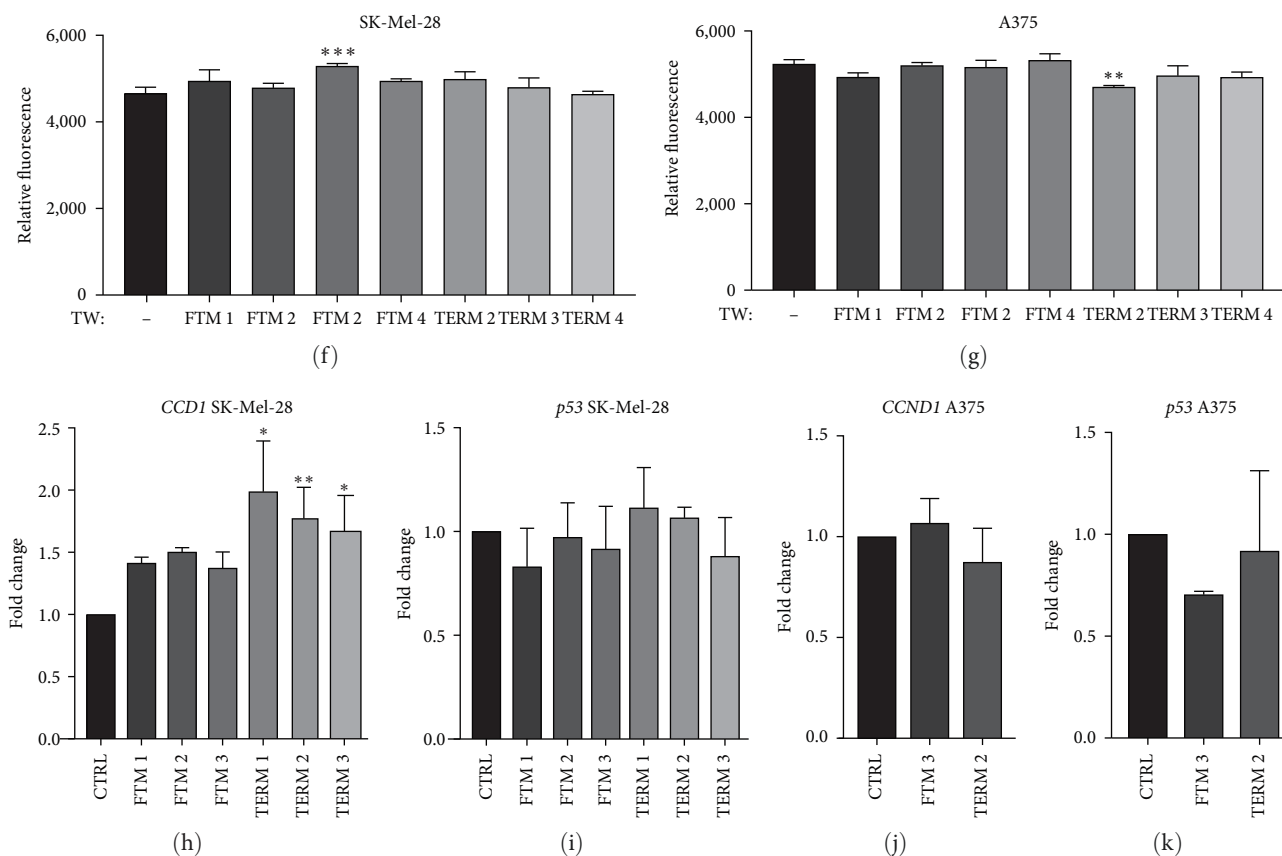

(d)

(e)

Figure 7: Continued.

Figure 7: HUCPVC indirect coculture with SK-Mel-28 and A375 melanoma cells. (a–e) 2×10^6 melanoma cells were seeded in bottom wells with 1.5×10^4 HUCPVC or media only (−) in transwells. CCK8 growth assays were performed at 72 hr for (b) SK-Mel-28 and (c) A375 melanoma cells. OD was measured at 450 nm. Data presented as fold change relative to control, $n = 3$ per group. LDH release from (d) SK-Mel-28 and (e) A375 cells at 72 hr was measured via cytotoxicity detection assay. OD was measured at 450 nm, $n = 3$ per group. (f and g) 1×10^6 (f) SK-Mel-28 or (g) A375 were seeded in serum-free media in Matrigel-coated transwells with bottom wells containing media only (−) or 1×10^4 HUCPVC. Cancer cells invading through Matrigel were stained with cell tracker green and invasion was assessed after 72 hr. Relative fluorescence was read to measure invasiness, $n = 3$ per group. (h–k) After 120 hr in indirect coculture with HUCPVC, SK-Mel-28 expression of (h) CCND1 and (i) p53 and A375 expression of (j) CCND1 and (k) p53 were measured. Data presented as fold change relative to untreated control cells, $n = 3$ per group. $*p < 0.05$, $**p < 0.01$, $***p < 0.001$. Error bars represent SD. Scare bar = 125 microns.

vitro and *in vivo* experiments, possibly due to differences in our MSC delivery approach and in the timing of our assays. While the goal of our study was to assess the safety of HUCPVC injected systemically, the most frequently used MSC delivery approach in clinical trials [34], we were surprised to observe antitumor effects given the well known proregenerative capacities of HUCPVC. Further studies are required to fully leverage and understand the anticancer properties of HUCPVC administered IV.

Other studies have reported that mouse BM-MSC injected IV 24 hr posttumor induction in a mouse melanoma tumor-bearing immunocompetent model, elicit an antitumor effect, while MSCs injected 14 days posttumor induction result in a protumor effect [35]. The tumor microenvironment is thought to play a role in modulating the effect of MSC treatment. During the early stages of melanoma growth, the tumor microenvironment is enriched with NK and T cells, while the late tumor environment promotes immunosuppression and is permissive of tumor growth [35]. Since our experiments were conducted

with NOD SCID mice lacking B and T cells, and have deficient innate immune cells, the tumor microenvironment differs significantly from that of an immunocompetent mouse model. As such, further experimental approaches that are compatible with the use of immunocompetent mice or alternate immunocompromised mouse models may be warranted to further assess the immunomodulatory responses elicited by HUCPVC treatment, and the ultimate impact this has on tumor cell populations. We have shown that the systemic delivery of HUCPVC leads to a rapid accumulation of cells in the lungs, resulting in long-lasting anti-inflammatory effects in immunocompetent models [8, 26], and the same was observed (decrease in TNF-α serum levels and CRP) at the 2- and 3-week time points following injection in a NOD SCID model. A similar proportion of macrophage cells were detected in the lung and liver of NOD SCID mice 24 hr after injection as we have reported in previous studies [26], suggesting that this may be a conserved response linked to immunomodulation following IV HUCPVC treatment. Our *in vivo* experiments demonstrate that HUCPVC delivered
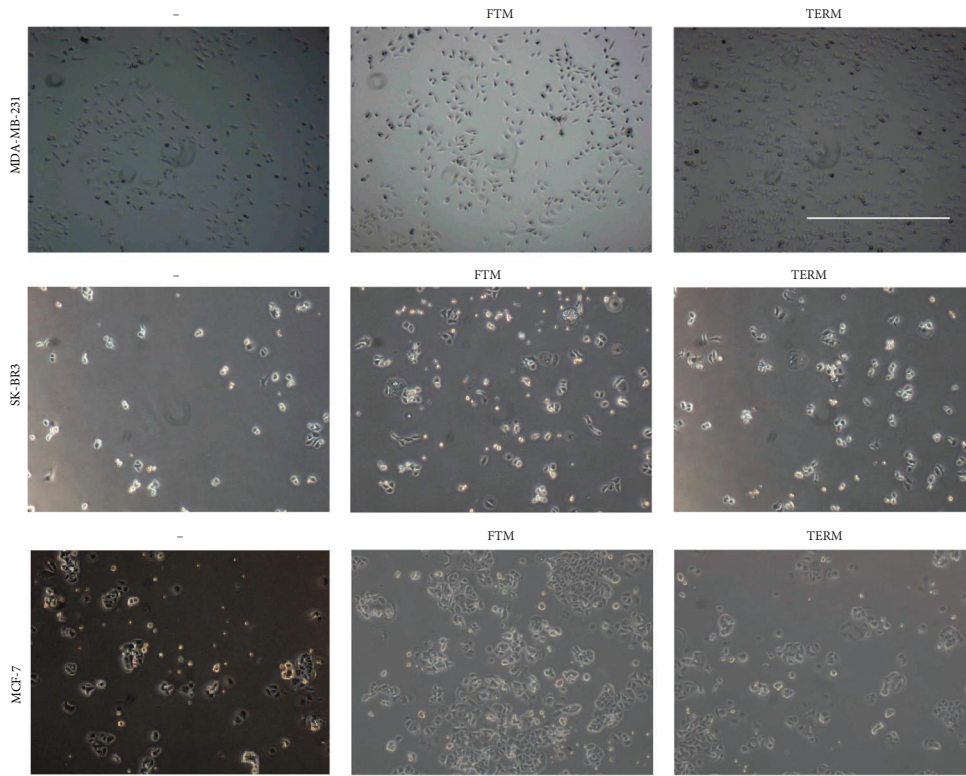
(a)
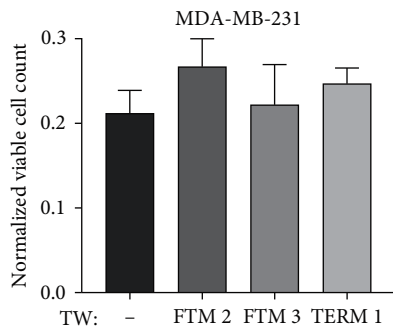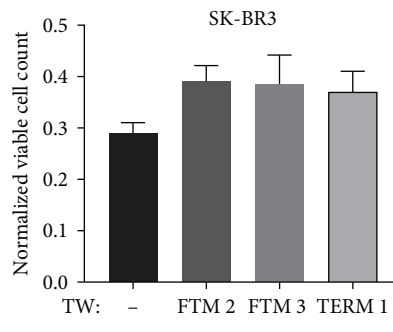
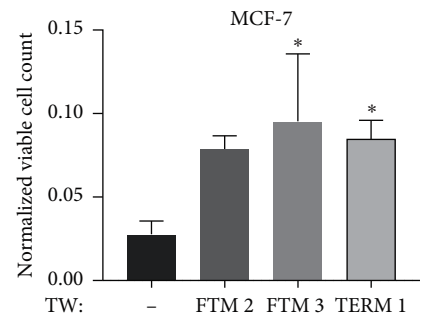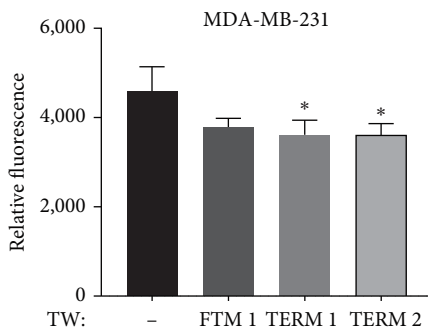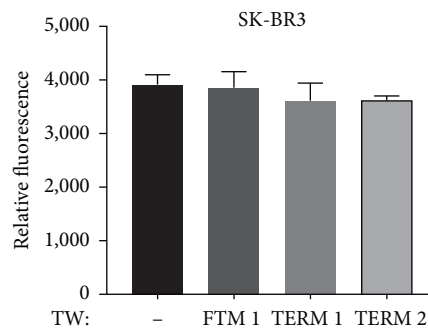(b)   (c)   (d)
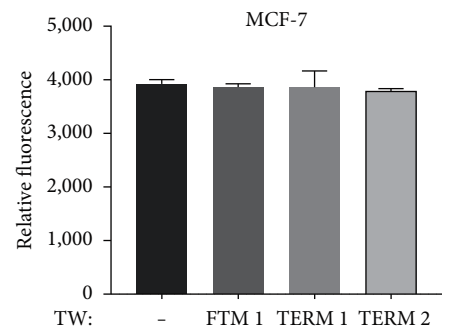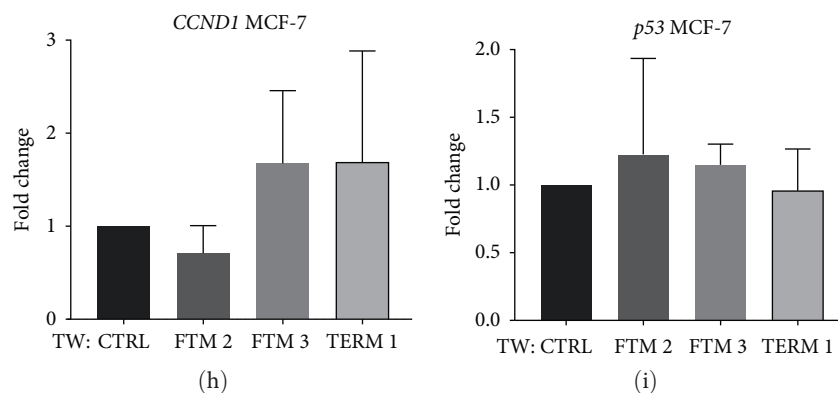

(e)   (f)   (g)

FIGURE 8: Continued.

FIGURE 8: HUCPVC indirect coculture with MDA-MB-231, SKBR3, and MCF7 breast cancer cells. (a–d) 1.5×10^4 breast cancer cells were seeded in bottom wells with 2×10^6 HUCPVC or media only (−) in transwells. CCK8 growth assays were performed at 48 hr for (b) MDA-MB-231, (c) SKBR3, and 72 hr for (d) MCF7. OD was measured at 450 nm, $n = 3$ per group. (e–g) 1×10^6 (e) MDA-MB-231, (f) SKBR3, or (g) MCF7 breast cancer cells were seeded in serum-free media in Matrigel-coated transwells with bottom wells containing media only (−) or 1×10^4 HUCPVC. Cancer cells invading through Matrigel were stained with cell tracker green and invasion was assessed after 72 hr. Relative fluorescence was read to measure invasiness, $n = 3$ per group. (h and i) After 120 hr in indirect coculture with HUCPVC: (h) CCND1 and (i) p53 expression by MCF7 breast cancer cells were measured. Data presented as fold change relative to untreated control MCF7 cells, $n = 3$ per group. $^*p < 0.05$. Error bars represent SD. Scare bar = 125 microns.

systemically do not actively home to tumors, which suggests that the inhibitory effect they have on tumor growth is likely to be largely a systemic endocrine effect rather than occurring by a localized paracrine mechanism [8]. The colocalization of HUCPVC with macrophages in the lungs and liver, as observed in other models in our lab previously [8, 19, 26], indicates a potential role for HUCPVC in regulating immune cells and inflammation. Our initial investigations on M2 macrophage markers do not support an effect on macrophage polarization in this model, at least not at the time points investigated. Few HUCPVC-derived qdots were found in the tumor at 24 hr and 3-weeks postinjection, and the majority of those were not associated with macrophage markers, suggesting that systemic immunomodulatory effects and not homing of monocytes that phagocytosed HUCVPC are likely responsible for the effects on tumor growth.

HUCPVC do not appear to localize to tumor tissue in amounts that are sufficient to modulate tumor growth. However, given the discrepancies on the published effects of MSC on cancer cell growth, we investigated the effects of HUCPVCs on SK-MEL-28 melanoma cells and other melanoma and breast cancer cells in vitro to determine whether their paracrine properties could promote tumor growth, as an additional assessment of safety. We previously published that HUCPVC express and secrete factors such as fibroblast growth factors, bone morphogenetic proteins, vascular endothelial growth factor, and others that in many context have procell survival and proliferation effects [18, 20]. Overall, our in vitro results suggest that HUCPVC largely do not promote melanoma and breast cancer cell growth and may represent a safe and effective cell candidate for cancer patients in the presence of some tumor types, including those with properties similar to SK-MEL-28, but not all cancer types, including possibly some types of breast cancers that would share similar responses to the MCF-7 line. This in vitro work is an obvious simplification of an in vivo system, as it does not enable investigation of the role of the immune system or

supporting vasculature. In addition, it is a flawed system as the cells are each also impacted by growth factor uptake and waste released in the media, and culture conditions may alter the cell subpopulations. While the majority of HUCPVC lines showed neutral effects on cancer cells in our coculture model, some procancer effects were observed in A375 and MCF-7 lines and anticancer effects were observed in SKBR7, which appear to be HUCPCV line-dependent. Some of these differences, for example, the progrowth effects of two FTM lines on A375 versus neutral effects on SK-Mel-28 could be explained by the fact that the two melanoma cell lines have contrasting transcriptional profiles that are suggestive of the presence of more cells with increased levels of invasive gene transcripts in the former, and a more proliferative gene expression profile in the latter [36]. With regards to melanoma cells, the previous literature suggested that a line of umbilical cord (UC)-MSC could inhibit the proliferation, induce apoptosis, and suppress the invasion of A375 cells [37]. Such discordance and other comparisons between our findings and previous reports of similar studies assessing the effect of umbilical cord-derived MSC on melanoma and breast cancer cell lines [38–46] are summarized in Table S2. Discrepancies may be due, in part, to alternative methods for evaluating cancer cell proliferation, in addition to differing culture systems, or may be due to the heterogeneity in MSC lines utilized across various studies, as the present study would suggest. Future studies could investigate differences in the RNA expression profiles or secretomes of the HUCPVC lines and cancer cells to further understand their varying paracrine effects on tumor growth in vitro. However, given the limitations of in vitro coculture assays, single cell analyses of tumor cells and peripheral immune cells in various tumor-bearing animal models at various timepoints following HUCPVC injection would likely yield a more accurate understanding of the mechanisms that influence cell proliferation and tumor growth. Finally, the study sheds light on potential sources of discrepancy between various in vitro and

in vivo assays, including limitations of each, to assess the impact of HUCPVC and possibly other MSC on cancer cell proliferation and tumor growth.

5. Conclusions

HUCPVC therapy to prevent side effects of cancer treatments may be safe in the context of some cancers and may also have antitumor effects.

Data Availability

The analyzed data used to support the findings of this study are included in the manuscript or supplementary files, and data files are available from the corresponding author upon request.

Ethical Approval

This study was approved by the Animal Care Committee of the University Health Network (AUP grant number 5232). Independent research ethics board approval was obtained for the collection of first trimester human umbilical cords (REB grant number 28889, University of Toronto, Canada) and for ongoing investigations in preclinical research studies (VERITAS grant number 16540).

Consent

Written informed consent was obtained for each sample collection. Human umbilical cords from the first trimester (8-–12 weeks of gestation) were previously obtained from consenting patients who underwent elective pregnancy termination at an independent facility.

Conflicts of Interest

Dr. Clifford Librach holds patents in Canada, U.S., and Australia for the invention entitled "Method of Isolation and Use of Cells Derived from First Trimester Umbilical Cord Tissue". The other authors have no commercial, proprietary, or financial interest in the products or companies described in this article.

Authors' Contributions

Conception and design of the study: LL, DG, SM, AGF, and CLL. Acquisition of data: LL, EM, HSH, HK, AG, AU, BW, PM, MS, JF, AG, SM, and AK. Analysis and interpretation of data: LL, EM, HSH, HK, AG, SM, DG, AGF, and CLL. Drafting or revising the manuscript: LL, EM, HSH, HK, AGF, and CLL. All authors reviewed and approved the final article. Lianet Lopez, Hannah Shuster-Hyman, and Eden Marco, contributed equally to this study.

Acknowledgments

Supplementary Materials

Figure S1: phenotypic characterization of FTM HUCPVC (FTM 1, FTM 2). Figure S2: standard curve to validate cell counting assay linearity. Figure S3: representative flow cytometry dot plots for immune cell analysis in tumor model, and tabular analysis. Figure S4: colocalization of macrophage marker CD206 with Qdot at 24 hr and 3 weeks in tumor tissue following systemic injection in the NOD SCID SKMEL28 xenograft model. Figure S5: analysis of macrophage markers CD206 and CD68 at 24 hr in liver, lung, and tumor tissue following systemic injection in the NOD SCID SKMEL28 xenograft model. Table S1: qPCR primer sequences. Table S2: summary of *in vitro* studies to determine effect of FTM and term HUCPVC on breast cancer and melanoma cell lines. (*Supplementary Materials*)

References

[1] R. L. Siegel, K. D. Miller, H. E. Fuchs, and A. Jemal, "Cancer statistics, 2021," *CA: A Cancer Journal for Clinicians*, vol. 71, no. 2021, pp. 7–33, 2021.

[2] K. Nurgali, R. T. Jagoe, and R. Abalo, "Editorial: adverse effects of cancer chemotherapy: anything new to improve tolerance and reduce sequelae?" *Frontiers in Pharmacology*, vol. 9, Article ID 245, 2018.

[3] L. Kalich-Philosoph, H. Roness, A. Carmely et al., "Cyclophosphamide triggers follicle activation and "burnout"; AS101 prevents follicle loss and preserves fertility," *Science Translational Medicine*, vol. 5, no. 185, Article ID 185ra162, 2013.

[4] H. Sung, J. Ferlay, R. L. Siegel et al., "Global cancer statistics 2020: GLOBOCAN estimates of incidence and mortality worldwide for 36 cancers in 185 countries," *CA: A Cancer Journal for Clinicians*, vol. 71, no. 3, pp. 209–249, 2021.

[5] K. B. Reed, J. D. Brewer, C. M. Lohse, K. E. Bringe, C. N. Pruitt, and L. E. Gibson, "Increasing incidence of melanoma among young adults: an epidemiological study in Olmsted County, Minnesota," *Mayo Clinic Proceedings*, vol. 87, no. 4, pp. 328–334, 2012.

[6] M. Dominici, K. Le Blanc, I. Mueller et al., "Minimal criteria for defining multipotent mesenchymal stromal cells. The International Society for Cellular Therapy position statement," *Cytotherapy*, vol. 8, no. 4, pp. 315–317, 2006.

[7] R. M. Samsonraj, M. Raghunath, V. Nurcombe, J. H. Hui, A. J. van Wijnen, and S. M. Cool, "Concise review: multifaceted characterization of human mesenchymal stem cells for use in regenerative medicine," *Stem Cells Translational Medicine*, vol. 6, no. 12, pp. 2173–2185, 2017.

[8] D. Gallagher, F. Siddiqui, J. Fish et al., "Mesenchymal stromal cells modulate peripheral stress-induced innate immune activation indirectly limiting the emergence of neuroinflammation-driven

depressive and anxiety-like behaviors," *Biological Psychiatry*, vol. 86, no. 9, pp. 712–724, 2019.

[9] J. Zhang, L. Hou, D. Zhao et al., "Inhibitory effect and mechanism of mesenchymal stem cells on melanoma cells," *Clinical and Translational Oncology*, vol. 19, no. 11, pp. 1358–1374, 2017.

[10] H.-Y. Lee and I.-S. Hong, "Double-edged sword of mesenchymal stem cells: cancer-promoting versus therapeutic potential," *Cancer Science*, vol. 108, no. 10, pp. 1939–1946, 2017.

[11] C. Zhang, S.-J. Yang, Q. Wen et al., "Human-derived normal mesenchymal stem/stromal cells in anticancer therapies," *Journal of Cancer*, vol. 8, no. 1, pp. 85–96, 2017.

[12] J.-O. Ahn, Y.-R. Coh, H.-W. Lee, I.-S. Shin, S.-K. Kang, and H.-Y. Youn, "Human adipose tissue-derived mesenchymal stem cells inhibit melanoma growth in vitro and in vivo," *Anticancer Research*, vol. 35, no. 1, pp. 159–168, 2015.

[13] F. C. de Menezes, L. G. S. Cabral, M. C. Petrellis, C. F. Neto, and D. A. Maria, "Antitumor effect of cell therapy with mesenchymal stem cells on murine melanoma B16-F10," *Biomedicine & Pharmacotherapy*, vol. 128, Article ID 110294, 2020.

[14] D. Baksh, R. Yao, and R. S. Tuan, "Comparison of proliferative and multilineage differentiation potential of human mesenchymal stem cells derived from umbilical cord and bone marrow," *Stem Cells*, vol. 25, no. 6, pp. 1384–1392, 2007.

[15] N. Zebardast, D. Lickorish, and J. E. Davies, "Human umbilical cord perivascular cells (HUCPVC): a mesenchymal cell source for dermal wound healing," *Organogenesis*, vol. 6, no. 4, pp. 197–203, 2010.

[16] P. Szaraz, M. Librach, L. Maghen et al., "*In Vitro* differentiation of first trimester human umbilical cord perivascular cells into contracting cardiomyocyte-like cells," *Stem Cells International*, vol. 2016, Article ID 7513252, 13 pages, 2016.

[17] S.-H. Hong, L. Maghen, S. Kenigsberg et al., "Ontogeny of human umbilical cord perivascular cells: molecular and fate potential changes during gestation," *Stem Cells and Development*, vol. 22, no. 17, pp. 2425–2439, 2013.

[18] K. Zohni, L. Lopez, P. Mander et al., "Human umbilical cord perivascular cells maintain regenerative traits following exposure to cyclophosphamide," *Cancer Letters*, vol. 501, pp. 133–146, 2021.

[19] F. Siddiqui, D. Gallagher, H. Shuster-Hyman, L. Lopez, A. Gauthier-Fisher, and C. L. Librach, "First trimester human umbilical cord perivascular cells (HUCPVC) modulate the kynurenine pathway and glutamate neurotransmission in an LPS-induced mouse model of neuroinflammation," *Journal of Inflammation*, vol. 20, Article ID 15, 2023.

[20] F. Iqbal, A. Johnston, B. Wyse et al., "Combination human umbilical cord perivascular and endothelial colony forming cell therapy for ischemic cardiac injury," *npj Regenerative Medicine*, vol. 8, Article ID 45, 2023.

[21] E. Shlush, L. Maghen, S. Swanson et al., "In vitro generation of Sertoli-like and haploid spermatid-like cells from human umbilical cord perivascular cells," *Stem Cell Research & Therapy*, vol. 8, Article ID 37, 2017.

[22] L. Maghen, E. Shlush, I. Gat et al., "Human umbilical perivascular cells: a novel source of MSCs to support testicular niche regeneration," *Reproduction*, vol. 153, no. 1, pp. 85–95, 2016.

[23] J. Mashiach, L. Lianet, M. Filice et al., "Human umbilical cord perivascular cells (HUCPVC) prevent chemotherapeutic drug-induced male infertility in a mouse model," *F&S Science*, vol. 2, no. 1, pp. 24–32, 2020.

[24] F. Iqbal, Y. S. Gratch, P. Szaraz, and C. L. Librach, "The aortic ring co-culture assay: a convenient tool to assess the angiogenic potential of mesenchymal stromal cells in vitro," *Journal of Visualized Experiments*, no. 127, Article ID e56083, 2017.

[25] A. Gauthier-Fisher, A. Kauffman, and C. L. Librach, "Potential use of stem cells for fertility preservation," *Andrology*, vol. 8, no. 4, pp. 862–878, 2020.

[26] H. Shuster-Hyman, F. Siddiqui, D. Gallagher, A. Gauthier-Fisher, and C. L. Librach, "Time course and mechanistic analysis of human umbilical cord perivascular cell mitigation of lipopolysaccharide-induced systemic and neurological inflammation," *Cytotherapy*, vol. 25, no. 2, pp. 125–137, 2023.

[27] I. Nenu, D. Tudor, A. G. Filip, and I. Baldea, "Current position of TNF-α in melanomagenesis," *Tumor Biology*, vol. 36, no. 9, pp. 6589–6602, 2015.

[28] D. O'Brian, M. Prunty, A. Hill, and J. Shoag, "The role of C-reactive protein in kidney, bladder, and prostate cancers," *Frontiers in Immunology*, vol. 12, Article ID 721989, 2021.

[29] J. Dai, K. Tang, W. Xiao et al., "Prognostic significance of C-reactive protein in urological cancers: a systematic review and meta-analysis," *Asian Pacific Journal of Cancer Prevention*, vol. 15, no. 8, pp. 3369–3375, 2014.

[30] M. W. Socha, B. Malinowski, O. Puk et al., "C-reactive protein as a diagnostic and prognostic factor of endometrial cancer," *Critical Reviews in Oncology/Hematology*, vol. 164, Article ID 103419, 2021.

[31] T. Yoshida, J. Ichikawa, I. Giuroiu et al., "C reactive protein impairs adaptive immunity in immune cells of patients with melanoma," *Journal for ImmunoTherapy of Cancer*, vol. 8, no. 1, Article ID e000234, 2019.

[32] H. S. F. Shuster-Hyman, D. Gallagher, A. Gauthier-Fisher, and C. L. Librach, "Time course and mechanistic analysis of human umbilical cord perivascular Cell (HUCPVC) mitigation of LPS-induced systemic and neurological inflammation," *Cytotherapy*, 2022.

[33] M. Dviri, L. Lopez, M. Madjunkov et al., "Human umbilical cord perivascular cells (HUCPVC) reduce ovarian fibrosis and improve pregnancy rates in a mouse model of natural ovarian aging," *Human Reproduction*, vol. 38, no. Supplement_1, Article ID dead093.1107, 2023.

[34] M. Kabat, I. Bobkov, S. Kumar, and M. Grumet, "Trends in mesenchymal stem cell clinical trials 2004–2018: is efficacy optimal in a narrow dose range?" *Stem Cells Translational Medicine*, vol. 9, no. 1, pp. 17–27, 2020.

[35] D. Miloradovic, D. Miloradovic, B. S. Markovic et al., "The effects of mesenchymal stem cells on antimelanoma immunity depend on the timing of their administration," *Stem Cells International*, vol. 2020, Article ID 8842659, 13 pages, 2020.

[36] K. M. Vincent and L. M. Postovit, "Investigating the utility of human melanoma cell lines as tumour models," *Oncotarget*, vol. 8, no. 6, pp. 10498–10509, 2017.

[37] W. Wang, L. Li, F. Chen, and Y. Yang, "Umbilical cord-derived mesenchymal stem cells can inhibit the biological functions of melanoma A375 cells," *Oncology Reports*, vol. 40, pp. 511–517, 2018.

[38] K. Mandel, Y. Yang, A. Schambach, S. Glage, A. Otte, and R. Hass, "Mesenchymal stem cells directly interact with breast cancer cells and promote tumor cell growth in vitro and in vivo," *Stem Cells and Development*, vol. 22, no. 23, pp. 3114–3127, 2013.

[39] T. Li, C. Zhang, Y. Ding et al., "Umbilical cord-derived mesenchymal stem cells promote proliferation and migration

in MCF-7 and MDA-MB-231 breast cancer cells through activation of the ERK pathway," *Oncology Reports*, vol. 34, no. 3, pp. 1469–1477, 2015.

[40] P. Li, H. Zhou, G. Di et al., "Mesenchymal stem cell-conditioned medium promotes MDA-MB-231 cell migration and inhibits A549 cell migration by regulating insulin receptor and human epidermal growth factor receptor 3 phosphorylation," *Oncology Letters*, vol. 13, no. 3, pp. 1581–1586, 2017.

[41] K. Gauthaman, F. C. Yee, S. Cheyyatraivendran, A. Biswas, M. Choolani, and A. Bongso, "Human umbilical cord wharton's jelly stem cell (hWJSC) extracts inhibit cancer cell growth in vitro," *Journal of Cellular Biochemistry*, vol. 113, no. 6, pp. 2027–2039, 2012.

[42] N. He, Y. Kong, X. Lei et al., "MSCs inhibit tumor progression and enhance radiosensitivity of breast cancer cells by down-regulating Stat3 signaling pathway," *Cell Death & Disease*, vol. 9, Article ID 1026, 2018.

[43] M. Mirabdollahi, S. Haghjooyjavanmard, and H. Sadeghi-Aliabadi, "An anticancer effect of umbilical cord-derived mesenchymal stem cell secretome on the breast cancer cell line," *Cell and Tissue Banking*, vol. 20, no. 3, pp. 423–434, 2019.

[44] M. Mirabdollahi, H. Sadeghi-Aliabadi, and S. Haghjooy Javanmard, "Human Wharton's jelly mesenchymal stem cells-derived secretome could inhibit breast cancer growth *in vitro* and *in vivo*," *Iranian Journal of Basic Medical Sciences*, vol. 23, no. 7, pp. 945–953, 2020.

[45] F. Ma, D. Chen, F. Chen et al., "Human umbilical cord mesenchymal stem cells promote breast cancer metastasis by interleukin-8- and interleukin-6-dependent induction of CD44$^+$/CD24$^-$ Cells," *Cell Transplantation*, vol. 24, no. 12, pp. 2585–2599, 2015.

[46] R. Ayuzawa, C. Doi, R. S. Rachakatla et al., "Naïve human umbilical cord matrix derived stem cells significantly attenuate growth of human breast cancer cells in vitro and in vivo," *Cancer Letters*, vol. 280, no. 1, pp. 31–37, 2009.